Genetics in Medicine

Inherited duplications of PPP2R3B predispose to naevi and melanoma via a C21orf91-driven proliferative phenotype

--Manuscript Draft--

Manuscript Number:	GIM-D-20-00465R5
Article Type:	Article
Section/Category:	Clinical Genetics and Genomics
Corresponding Author:	Veronica A Kinsler, MD PhD Francis Crick Institute London, London UNITED KINGDOM
First Author:	Satyamaanasa Polubothu, MD PhD
Order of Authors:	Satyamaanasa Polubothu, MD PhD
	Davide Zecchin, PhD
	Lara Al-Olabi
	Daniël A Lionarons, MD PhD
	Mark Harland, PhD
	Stuart Horswell
	Anna C Thomas, PhD
	Lilian Hunt
	Nathan Wlodarchak, PhD
	Paula Aguilera
	Sarah Brand
	Dale Bryant, PhD
	Cristina Carrera
	Hui Chen, PhD
	Greg Elgar, PhD
	Catherine A Harwood
	Michael Howell, PhD
	Lionel Larue
	Sam Loughlin
	Jeff Macdonald
	Josep Malvehy, MD PhD
	Sara Barberan Martin, PhD
	Vanessa Martins da Silva, MD PhD
	Miriam Molina, PhD
	Deborah Morrogh, PhD
	Dale Moulding, PhD
	Jérémie Nsengimana, PhD
	Alan Pittman
	Joan-Anton Puig-Butillé

	Kiran Parmar
	Neil J Sebire, MD PhD
	Stephen Scherer
	Paulina Stadnik, PhD
	Phil Stanier, PhD
	Gemma Tell
	Regula Waelchli, MD
	Mehdi Zarrei, PhD
	Susana Puig, MD PhD
	Véronique Bataille, MD PhD
	Yongna Xing, PhD
	Eugene Healy
	Gudrun Moore
	Wei-Li Di, MD PhD
	Julia Newton-Bishop
	Julian Downward, MD PhD
	Veronica A Kinsler, MD PhD
Manuscript Region of Origin:	UNITED KINGDOM
Abstract:	Purpose Much of the heredity of melanoma remains unexplained. We sought predisposing germline copy number variants using a rare disease approach. Methods Whole genome copy number findings in patients with melanoma predisposition syndrome Congenital Melanocytic Naevus were extrapolated to a sporadic melanoma cohort. Functional effects of duplications in PPP2R3B were investigated using immunohistochemistry, transcriptomics, and stable inducible cellular models, themselves characterised using RNAseq, qRT-PCR, reverse phase protein arrays, immunoblotting, RNA interference, immunocytochemistry, proliferation and migration assays. Results We identify here a previously unreported genetic susceptibility to melanoma and melanocytic naevi, familial duplications of gene PPP2R3B. This encodes PR70, a regulatory unit of critical phosphatase PP2A. Duplications increase expression of PR70 in human naevus, and increased expression in melanoma tissue correlates with survival via a non-immunological mechanism. PPP2R3B overexpression induces pigment cell switching towards proliferation and away from migration. Importantly, this is independent of the known MITF-controlled switch, instead driven by C21orf91 . Finally, C21orf91 is demonstrated to be downstream of MITF as well as PR70. Conclusions This work confirms the power of a rare disease approach, identifying a previously unreported copy number change predisposing to melanocytic neoplasia, and discovers C21orf91 as a potentially targetable hub in the control of phenotype switching.

Title

Inherited duplications of *PPP2R3B* predispose to naevi and melanoma via a *C21orf91*-driven proliferative phenotype

Authors

Satyamaanasa Polubothu[1,2,3], Davide Zecchin[1,2], Lara Al-Olabi[2], Daniël A Lionarons[4], Mark Harland[5], Stuart Horswell[6] , Anna C Thomas[2], Lilian Hunt[7], Nathan Wlodarchak[8], Paula Aguilera[9], Sarah Brand[2], Dale Bryant[1,2], Cristina Carrera[9], Hui Chen[8], Greg Elgar[7], Catherine A Harwood[10], Michael Howell[11], Lionel Larue[12], Sam Loughlin[13], Jeff MacDonald[14], Josep Malvehy[9], Sara Martin Barberan[1,2], Vanessa Martins da Silva[2,9], Miriam Molina[4], Deborah Morrogh[13], Dale Moulding[2], Jérémie Nsengimana[5], Alan Pittman[15], Joan-Anton Puig-Butillé[9], Kiran Parmar[16], Neil J Sebire[17], Stephen Scherer[14], Paulina Stadnik[2], Philip Stanier[2], Gemma Tell[8], Regula Waelchli[3], Mehdi Zarrei[14], Susana Puig[9], Véronique Bataille[15], Yongna Xing[8], Eugene Healy[18], Gudrun E Moore[2], Wei-Li Di[19], Julia Newton-Bishop[5], Julian Downward[4], Veronica A Kinsler[1,2,3]*

Affiliations

1 Mosaicism and Precision Medicine Laboratory, Francis Crick Institute, London, UK

2 Genetics and Genomic Medicine, UCL GOS Institute of Child Health, London, UK.

3 Paediatric Dermatology, Great Ormond Street Hospital for Children, London, UK.

4 Oncogene Biology Laboratory, Francis Crick Institute, London, UK.

5 Section of Epidemiology and Biostatistics, Leeds Institute of Cancer and Pathology, Cancer Research UK Clinical Centre at Leeds, St James's University Hospital, Leeds, UK.

6 Bioinformatics and Biostatistics, Francis Crick Institute, London, UK.

7 Advanced Sequencing Facility, Francis Crick Institute, London, UK.

[8] McArdle Laboratory, Department of Oncology, University of Wisconsin-Madison, School of Medicine and Public Health, Madison, WI, USA.

[9] Department of Dermatology, Hospital Clínic de Barcelona (Melanoma Unit), University of Barcelona, IDIBAPS, Barcelona & CIBERER, Barcelona, Spain.

[10] Centre for Cell Biology and Cutaneous Research, Blizzard Institute, Barts, London, United Kingdom.

[11] High Throughput Screening Facility, Francis Crick Institute, London.

[12] Centre de Recherche, Developmental Genetics of Melanocytes, Institut Curie, Orsay, France.

[13] North East Thames Regional Genetics Laboratory Service, Great Ormond Street Hospital for Children NHS Foundation Trust, London, United Kingdom.

[14] The Centre for Applied Genomics and Program in Genetics and Genome Biology, The Hospital for Sick Children, Toronto, Ontario, Canada.

[15] Bioinformatics, St George's University of London, London, UK.

[16] Department of Twin Research and Genetic Epidemiology, King's College London, South Wing Block D, Westminster Bridge Road, London SE1 7EH, UK.

[17] Department of Histopathology, Great Ormond Street Hospital for Children, London, UK.

[18] Department of Dermatology, University Hospital Southampton NHS Foundation Trust, Southampton, UK.

[19] Infection, Immunity and Inflammation Programme, Immunobiology Section, UCL GOS Institute of Child Health, London, United Kingdom.

Corresponding author

Veronica Kinsler, The Francis Crick Institute, 1 Midland Rd, London NW1 1AT; veronica.kinsler@crick.ac.uk

Abstract

Purpose

Much of the heredity of melanoma remains unexplained. We sought predisposing germline copy number variants using a rare disease approach.

Methods

Whole genome copy number findings in patients with melanoma predisposition syndrome Congenital Melanocytic Naevus were extrapolated to a sporadic melanoma cohort. Functional effects of duplications in *PPP2R3B* were investigated using immunohistochemistry, transcriptomics, and stable inducible cellular models, themselves characterised using RNAseq, qRT-PCR, reverse phase protein arrays, immunoblotting, RNA interference, immunocytochemistry, proliferation and migration assays.

Results

We identify here a previously unreported genetic susceptibility to melanoma and melanocytic naevi, familial duplications of gene *PPP2R3B.* This encodes PR70, a regulatory unit of critical phosphatase PP2A. Duplications increase expression of PR70 in human naevus, and increased expression in melanoma tissue correlates with survival via a non-immunological mechanism. *PPP2R3B* overexpression induces pigment cell switching towards proliferation and away from migration. Importantly, this is independent of the known MITF-controlled switch, instead driven by *C21orf91*. Finally, C21orf91 is demonstrated to be downstream of MITF as well as PR70.

Conclusions

This work confirms the power of a rare disease approach, identifying a previously unreported copy number change predisposing to melanocytic neoplasia, and discovers *C21orf91* as a potentially targetable hub in the control of phenotype switching.

Introduction

Melanoma (CMM [MIM:155600]) remains a major cause of morbidity and mortality. The majority of the heredity of melanoma remains unexplained, with germline variants in *CDKN2A* in 2% of cases the commonest known genetic predisposer[1]. Identification of new susceptibility genes is desirable to improve understanding of the condition at molecular level, with a view to better therapeutic options. We sought to identify novel susceptibility loci for melanocytic neoplasia, using a rare disorder approach.

Congenital melanocytic naevi (CMN [MIM 137550]) is a rare mosaic disorder of large and multiple moles, which predisposes affected individuals to melanoma. It is a valuable UV-independent genetic model for the development of melanoma, with causative somatic pathogenic variants in *NRAS* in 70%[2,3], and *BRAF* in 7%[3,4], with the remainder as yet unknown. Despite the sporadic somatic nature of the disease, one third of cases have a first or second degree family history of CMN in the largest published cohort[5,6], suggesting germline susceptibility to *NRAS*/*BRAF* somatic pathogenic variant in affected families, including the already established variants in *MC1R*[6]. We hypothesised that new predisposing copy number variants found via this rare disorder could also predispose to melanoma in the normal population.

Germline copy number in the CMN cohort was measured using an unbiased whole genome approach, and relevant findings validated in an adult melanoma cohort. Previously unreported duplications of gene *PPP2R3B* were discovered in both cohorts, at a frequency comparable to that of pathogenic *CDKN2A* variants. Extensive modelling of the biology of *PPP2R3B* overexpression demonstrated promotion of proliferation and reduction of migration in melanoma cells. The balance between proliferation and migration/invasion is

known as pigment cell phenotype switching, and its regulation is recognised as critical in melanoma progression and treatment[7,8]. This process was, surprisingly, independent of the key regulator of pigment cell phenotype switching, microphthalmia-associated transcription factor (MITF)[8,9]. Whole genome RNAseq instead revealed that *PPP2R3B* overexpression drives pigment phenotype switching via largely uncharacterised gene *C21orf91*. Moreover, MITF-driven proliferation in melanoma cells is rescuable by *C21orf91* knockdown, indicating that C21orf91 is downstream of both PR70 and MITF in our *in vitro* system, and as such is a potentially targetable hub in melanoma.

Materials and Methods

For methods of patient recruitment, ethical approvals, immunohistochemistry, immunocytochemistry, qRT-PCR, Western blotting, sample preparation, and all methods relating to supplementary results figures, please see **Supplementary Material.**

Array CGH

Whole genome array comparative genomic hybridization (CGH) was performed as per the manufacturer's instructions on 24 germline DNA samples from the CMN cohort, using Roche Nimblegen 135K oligonucleotide arrays and sex-matched commercial pooled controls. 1-3 µg of patient DNA and control DNA (Megapool reference DNA, Male – EA-100M, Female – EA-100F, Kreatech, The Netherlands) was labelled using NimbleGen Dual-Color DNA Labeling Kit and hybridized to the oligonucleotide array using the NimbleGen Hybridization System. Two-color array scanning was performed using a Molecular Devices GenePix 4400A (Molecular Devices inc, Sunneyville, CA, USA) at a resolution of 2.5 microns. Data were extracted using Deva software (NimbleGen), and analysed using InfoQuant CGHFusion (version 5.7.0 - 6.1.0) or later Chromosome Analysis Suite 4.0 (ChAS 4.0, Thermofisher Scientific). Abnormal copy number was called as per diagnostic facility criteria: at least 3 consecutive probe points above or below the zero line, with an average ratio of difference in fluorescence at least +/- 0.4 in those points, and excluding areas where CNVs had already been reported.

Targeted Next Generation Sequencing Panel

A SureSelect targeted panel (Agilent Technologies, UK) was designed to capture the whole genomic region encompassing the telomeric 4 genes on the pseudoautosomal region of X and Y chromosomes, chrX:198061-607558 chrY:148061-557558 (hg19/GRCh37). Library preparation was by SureSelectXT kit under manufacturer's instructions (Agilent Technologies, UK), and sequencing on NextSeq instrument 500/550, read length of 2x150 bp (Illumina, USA); Leeds melanoma samples (n= 168) and GOSH CMN samples (n=5). BAM files were inputted to DeepTools MultiBamSummary using the PPP2R3B_Moderately_Stringent_1_covered.bed probe coordinates file. Coverage across probe regions within hg19 coordinates were extracted and averaged. Three control samples were used to create 'normal expected' coverage ratios of the genes compared to *SHOX*. All samples were normalised compared to

these ratios and R studio was used to visualise and calculate gene coverage data across all samples.

Generation of stable inducible *PPP2R3B* cell lines

SKMEL2 and SKMEL30 melanoma cell lines carry variants affecting codon 61 of NRAS, and were cultured as per manufacturers' instructions. Normal *PPP2R3B* copy number in both cell lines was verified by NGS. Human *myc*-FLAG tagged *PPP2R3B* ORF clone from Origene *(*RC222908) was linearised and the insert DNA amplified using modified primers generating an N-terminal Myc tag. The In-Fusion® HD Cloning system (Takara, 638909) was used to allow directional cloning of the *PPP2R3B* insert into the AgeI-MluI site of the lentiviral vector pTRIPZ (GE Healthcare) resulting in the final *PPP2R3B* (tet-ON) construct, without the TurboRFP or shRNAmir-related elements of the parental pTRIPZ plasmid. Transduction of HEK 293T cells with pTRIPZ-*PPP2R3B* in addition to psPAX2 and pMD2.G lentiviral plasmids using Lipofectamine 2000™ generated lentiviral particles used to infect SKMEL2 or SKMEL30 target cells using polybrene to enhance efficiency. Stable cell lines were selected using puromycin.

Reverse Phase Protein Array

Protein samples were diluted to 1.5µg/µl and submitted to MD Anderson, Core Facility. Reported intensity values were log transformed to approximate normality and comparisons were performed using an un-paired t-test.

RNAseq

RNA integrity was assessed using a Bioanalyser (Agilent). Library preparation using KAPA mRNA HyperPrep Kit (Roche) was automated using the Hamilton robot, and sequenced using a NextSeq 500 (Illumina, San Diego, US) with a 43-bp paired-end run. Data were trimmed for 3' adapter sequences using Cutadapt 1.9.1, after which they were aligned to the Ensembl GRCh38 release 86 human transcriptome using STAR 2.5.2a. Individual lane level replicates were merged using Samtools 1.8, raw gene counts estimated using RSEM 1.3.0, and normalisation and differential expression called using DESeq2. A corrected p-value of <0.05 was deemed significant. Pathway analyses based on genes reported in the various analyses were performed using Metacore (Clarivate Analytics).

Proliferation Assays

WST1 proliferation Assay

SKMEL2-pTRIPZ-PPP2R3B and SKMEL30-pTRIPZ-PPP2R3B cells were seeded into a 96 well plate at a density of 1 x 10^4 cells/well. *PPP2R3B* overexpression was induced alongside un-induced controls. Plates were incubated for 48 hours at 37°C, prior to addition of WST-1 reagent. Plates were incubated in the dark at 37°C for two hours. Absorbance was read by spectrophotometer at 450nm and 620nm, adjusted for absorbance of blank media and of WST1 dye (620nm), and averaged across replicates (mean+SD). Significance was calculated by Students' t-test.

BrDU Proliferation Assay

BrdU Cell Proliferation ELISA Kit, (Abcam, ab126556) was used as per the manufacturer's instructions. SKMEL2-pTRIPZ-PPP2R3B and SKMEL30-pTRIPZ-PPP2R3B cells were seeded into a 96 well plate at a density of 2 x 10^5 cells/well, *PPP2R3B* overexpression induced alongside un-induced and suggested assay controls. Absorbance was averaged across replicates (mean+SD) and significance calculated by Students' t-test.

PPP2R3B overexpression IncuCyte® Cell Count Proliferation Assay

SKMEL2-pTRIPZ-PPP2R3B and SKMEL30-pTRIPZ-PPP2R3B cells were seeded into a 96-well ImageLock plate at a density of 1 x 10^4 cells/well. *PPP2R3B* overexpression was induced alongside un-induced control, a total of 12 replicates per condition. IncuCyte® live-cell analysis acquired 10X phase contrast images at a scanning interval of 60 minutes for 5 days, measuring percentage confluence. Confluence was averaged across replicates (mean+SD) and significance was calculated by Students' t-test.

C21orf91 Knockdown

The efficacy of three *C21orf91* siRNAs (Origene, SR310041) was assessed in cell line SKMEL2 at concentrations of 1nM, 5nM, 10nM and 25nM, and knockdown confirmed by qRT-PCR and Western blotting **(Figure S7)**. SKMEL2-pTRIPZ-PPP2R3B were seeded into a 96 well ImageLock plate at a density of 1 x 10^4 cells/well, one plate for the proliferation and one for the ScratchWound assay. *PPP2R3B* overexpression was induced alongside un-induced controls,

12 replicates per condition. Cells were transfected with Lipofectamine™ RNAiMAX using one or two *C21orf91* siRNAs or a scrambled siRNA (Origene, SR310041) at a concentration of 10nm. For the ScratchWound assay WoundMaker™ created a scratch in each well. Plates were washed with PBS and fresh media added. IncuCyte® live-cell analysis system acquired 10X phase contrast images at a scanning interval of 60 minutes for 5 days, for the proliferation assay and for 3 days for the ScratchWound assay. Confluence was averaged across replicates (mean+SD) and significance calculated by Students' t-test. Relative wound confluence was averaged across replicates (mean+SD) and significance calculated by Students' t-test.

***MITF* Knockdown and overexpression**

Cells were transfected with Lipofectamine™ RNAiMAX using two *MITF* siRNAs (siMITF 1: AAAGCAGTACCTTTCTACCAC; siMITF 2: TGGCTATGCTTACGCTTAA[43] or scrambled siRNA at a concentration of 25nm and knock-down was confirmed by qRT-PCR.

MITF overexpression was obtained by transiently transfecting cells with Lipofectamine 2000 and pCMV-TAG4A-MITF-M-wt plasmid (Addgene cat. 31151). Empty control vector was obtained by excision of *MITF* coding sequence from pCMV-TAG4A-MITF-M-wt plasmid (EcoRI and MfeI combined digestion) and ligation of compatible ends. Overexpression was confirmed through comparison by qRT-PCR of MITF-transfected and control vector-transfected cells.

Scratch Wound Assay

SKMEL2-pTRIPZ-PPP2R3B and SKMEL30-pTRIPZ-PPP2R3B cells were seeded into a 96-well ImageLock plate at a density of 1 x 10^5 cells/well. *PPP2R3B* overexpression was induced alongside un-induced controls, 12 replicates per condition, and plates incubated at 37 degrees until all wells were confluent. WoundMaker™ created a scratch in each well. Plates were washed with PBS and fresh media added. IncuCyte® live-cell analysis system acquired 10X phase contrast images at scanning intervals of 60 minutes. Relative wound confluence was averaged across replicates (mean+SD) and significance calculated by Students' t-test.

Leeds Melanoma Cohort – Transcriptomic data

Whole transcriptomes were derived from 703 FFPE primary cutaneous melanomas from the Leeds Melanoma Cohort[15] (median follow-up 7.5 years) using the Illumina DASL HT12.4 array. Kaplan-Meier survival analysis used melanoma specific survival (MSS), after correction for known confounding factors age, sex, AJCC (American joint committee for cancer) stage, vascular invasion, site, *BRAF/NRAS* pathogenic variant status and tumour invading lymphocytes (TILs).

Results

Germline duplications involving *PPP2R3B* are found at increased frequency in individuals with melanocytic neoplasia

Using whole genome array comparative genomic hybridisation (CGH) of leukocyte DNA, duplications of Xpter were identified in 3/24 (12.5%) randomly-selected patients with CMN, where only gene *PPP2R3B* was common to all three (**Figure 1a**). These three patients had causative post-zygotic pathogenic variants affecting codon 61 of *NRAS* in two cases, and no identified causative pathogenic variants (non-*NRAS,* non-*BRAF)* in the third. No other undescribed copy number variant was seen in more than one patient. Control data from paediatric patients with other phenotypes from the same diagnostic testing facility identified duplications of this gene (with or without involvement of the two telomeric genes but not extending centromeric) in only 13/4800, or 0.271%. Population data from normal individuals from the Database of Genomic Variants[10] identified similar duplications in only 1/36,000, or 0.003%[11], and 0.5% in nearly 7000 individuals in the MSSNG autism study[12,13], with no difference between cases and controls (personal communication). High-depth targeted next generation sequencing (NGS) was eventually selected as the most robust readout for copy number in this repetitive GC-rich telomeric region. NGS confirmed the CMN array findings and on screening leukocyte DNA from an adult sporadic melanoma cohort, identified the same germline duplications in 4/168 (2.4%), (all *BRAF* p.V600E), (**Figure 1b**), demonstrating that this copy number variant is enriched in populations with melanocytic neoplasia. Custom-designed multiple ligation-dependent probe amplification (MLPA, MRC Holland) validated the array-CGH findings and suggested the prevalence of duplications involving *PPP2R3B* to be 5% of the total cohort of 125 individuals with CMN (**Figure 1c,d**), but was not as robust as CGH or NGS for duplication discovery. Regional similarity search across Xp22.33 revealed three

segmental duplications 5' of *PPP2R3B*, and a high density of SINE and LINE repeats, but no segmental duplications between *PPP2R3B* and *SHOX* (**Figure 1e**). Sanger sequencing of leukocyte DNA from 48 CMN patients and 48 normal controls did not detect any unreported variants or haplotype differences (data not shown).

Germline duplications of *PPP2R3B* lead to increased expression of PR70 in congenital melanocytic naevi

Owing to other potential genetic confounders within malignant tissue such as loss of Xp, effects of germline duplication on tissue expression *in vivo* was visualised by immunohistochemistry in CMN tissue, known to have little somatic copy number variation[14]. Germline duplications were clearly associated with increased expression of PR70 in the available CMN tissue on immunohistochemistry compared to controls (**Figure 2a-f**).

Expression of PR70 is significantly associated with prolonged melanoma-specific survival (MSS)

Using published data of whole genome transcriptomic profiling of 703 melanomas[15], increased tissue expression of *PPP2R3B* was significantly associated with prolonged melanoma-specific survival (MSS) (**Figure 2g,h**). This effect remained significant after correction for known associations with survival, namely age, sex, AJCC (American joint committee for cancer) stage, vascular invasion, site, *BRAF/NRAS* pathogenic variant status and tumour invading lymphocytes (TILs). Unlike many known expression-survival associations in melanoma, transcriptomic pathway analysis did not support an immune pathway-mediated effect (**Figure 2i, Tables S3-S4**), leading us to look for an alternative mechanism of action of *PPP2R3B* overexpression on melanocytic proliferation.

Creation of a stable inducible overexpression system to study *PPP2R3B* overexpression.

The effects and mechanisms of *PPP2R3B* overexpression were modelled in detail by creation of a stable inducible over-expression system in two *NRAS*-mutant melanoma cell lines SKMEL2 and SKMEL30 (**Figure 3a-c**). Induction robustly and reproducibly led to *PPP2R3B* mRNA overexpression, and PR70 protein overexpression (antibody validated by CRISPR/Cas9 knockout, **Figure S6**).

***PPP2R3B* overexpression leads to increased cellular proliferation and decreased migration in 2D melanoma cell models**

Overall *PPP2R3B* overexpression led to pigment cell phenotype switching. This was measurable via significantly increased cellular proliferation by several alternative established methods, with some variation between cell lines (**Figure 3d-i**), and decreased migration in

scratch assays coupled to IncuCyte® monitoring (**Figure 3j-l**). siRNA knockdown of *PPP2R3B* did not alter proliferation (**Figure S7**), in line with the clinical data demonstrating duplications but not deletions in melanocytic neoplasia cohorts.

PPP2R3B overexpression does not significantly alter known melanoma signaling pathway activation

RNA sequencing pathway enrichment analysis identified suppression of the unfolded protein response and endoplasmic reticulum (ER) protein folding after induction of *PPP2R3B* (**Table S5**). Signaling pathway characterisation of 302 proteins using reverse phase protein arrays (RPPA, MD Anderson Core) pre- and post-induction of *PPP2R3B* demonstrated enrichment for mammalian target of rapamycin (mTOR) and hypoxia-induced factor 1 (HIF-1) signaling pathways, with prominent biological signatures of response to heat and stress (**Figure 4a-d, Table S6**). Immunoblotting provided validation of significantly decreased phosphorylation of AKT at 6-8 hours, however overall no dramatic effects on known melanoma signaling pathways were demonstrated (**Figure S3a-g**). Activation of CDC6, a known direct target of PR70[16], was inconsistent across cell lines (**Figure S3f,g**).

The ratio of PR70 to core PP2A enzyme appears to be critical

Increasing molar concentrations of PR70 up to a 1:1 ratio with that of the core PP2A enzyme increased PP2A activity towards its specific substrate pCDC6 in another cellular model, however, further increases in concentration reduced phosphatase activity (**Figure S4**). PR70 was shown to be highly efficient at binding to the PP2A core enzyme when competing with another regulatory subunit B'γ1, and overexpression of V5-tagged PR70 in a mammalian cell

line (C6) did not lead to free PR70 (**Figure S5**), suggesting either competitive binding of other PP2A holoenzymes or direct interactions with other effectors.

PPP2R3B overexpression leads to a significant and sustained rise in expression of previously uncharacterized gene *C21orf91*

Given the lack of clear signaling pathway activation in the presence of a pro-proliferative anti-migration phenotype, an alternative candidate mediator was sought by unbiased methods. Relatively unknown gene *C21orf91* (Refseq Gene ID:54149) was identified by RNA sequencing as the most significantly differentially-expressed gene in both cell lines, and validated at mRNA and protein levels (antibody validated by CRISPR/Cas9 knockout) (**Figure 4e,f, Table S7**). Knockdown of *C21orf91* by siRNA rescued both the increased proliferation and decreased migration and measured by Incucyte in SKMEL2 associated with induction of *PPP2R3B* expression (**Figure 5a-d**), firmly tying *C21orf91* to the phenotype switch.

PPP2R3B-induced *C21orf91*-driven pigment cell phenotype switching is independent of MITF

Importantly, the *PPP2R3B*-induced increase in *C21orf91* expression was independent of MITF, master regulator of melanocyte transcription and phenotype switching, as witnessed by the lack of MITF overexpression at mRNA and protein levels upon induction of *PPP2R3B* (**Figure S2**).

C21orf91 expression is positively correlated with *MITF* expression in melanoma

Given that MITF is the known master regulator of pro-proliferative phenotype switching in melanoma, and given that the pro-proliferative effect of C21orf91 was not mediated by MITF,

we hypothesised that C21orf91 could be an undescribed hub controlling pigment cell phenotype switching, and could therefore be downstream of MITF as well as downstream of PR70. In support, *C21orf91* and *MITF* expression were found to be significantly positively correlated in independent transcriptomic datasets from both melanoma cell lines and the melanoma patient cohort (**Figure S9a-d**), implying at least a key role for *C21orf91* in the pro-proliferative state of melanoma, and potentially that *MITF* can operate via *C21orf91*. *MITF* dependency score and *C21orf91* expression were also found to be significantly associated in melanoma cell lines **(Figure 5h)**, data extracted from the Cancer dependency Map (Broad Institute)[17-20]. Interestingly, *C21orf91* expression was not positively associated with *PPP2R3B* expression in the same two transcriptomic datasets, with association absent in one and negative in the other.

C21orf91 expression is regulated by MITF, and mediates MITF-induced proliferation

Knockdown of *MITF* led to decreased expression of *C21orf91* in SKMEL2 cell lines at baseline, demonstrating that *C21orf91* expression can also be regulated by *MITF* **(Figure 5e)**. Furthermore, increased proliferation in SKMEL2 cells over a five-day Incucyte experiment driven by overexpression of MITF was rescued by knockdown of *C21orf91* **(Figure 5f,g)**. C21orf91 is therefore a critical molecule controlling proliferation of melanoma cells from at least two pathways, one of which is the canonical pigment-cell phenotype switching pathway driven by MITF.

PR70 and C21orf91 are expressed throughout the cytoplasm, and their distribution was unchanged by *PPP2R3B* overexpression

PR70 subcellular localization by confocal microscopy was pan-cytoplasmic, including but not restricted to endoplasmic reticulum as previously suggested and not nucleoplasmic as currently suggested[21], and increased but unaltered in distribution by overexpression (**Figure 5i).** *C21orf91* expression was also demonstrated throughout the cytoplasm, and both PR70 and C21orf91 were increased in cells with two nuclei (**Figure 5i**).

Discussion

Copy number in the genome has in general been less systematically explored than sequence variation due to technical constraints[22], as copy number variation is enriched in areas of low genome mappability[23]. However, copy number variants (CNVs) are known to be prevalent in genes for cell communication and RAS-pathway signaling, including serine threonine kinases and phosphatases[24], and may therefore be highly relevant in the development of melanoma. Indeed, recent data on rare germline copy number variants affecting known melanoma susceptibility loci have demonstrated clear proof of concept of CNV predisposition in melanoma families[25]. Using a rare disease cohort, we identify here new germline duplications in the pseudoautosomal region 1 of the X chromosome which predispose to melanocytic neoplasia. Common to all was *PPP2R3B,* which encodes PR70, ubiquitously expressed in the cytoplasm, and one of the ß" family of regulatory units of the critical phosphatase and regulator of the cell cycle PP2A[26,27]. PP2A is a heterotrimeric holoenzyme consisting of a structural A subunit, a catalytic C subunit, and a regulatory B subunit[26,28]. The numerous non-homologous regulatory subunits are classified into B, B', B'' and B''' subfamilies, implicated in control of enzyme activity and substrate specificity[26,29]. PP2A operates via key effector

pathways RAS/MAPK, Wnt and AKT/mTOR[26,27]. As such, PP2A activity is intimately involved in malignancy and response to treatments[30], and is a major focus of potential therapeutics[30-33].

Analysis of the TCGA database demonstrates that copy number variants including *PPP2R3B* are more common across cancers in general than single nucleotide variants, suggesting that dosage of *PPP2R3B* is relevant in cancer development. In support of these data, a comprehensive study of the role of *PPP2R3B* expression in melanomas at tumour as opposed to germline level found the region to be copy-number sensitive, with loss of the inactivated X in females and decreased expression in males linked to decreased distant metastasis-free survival. The authors proposed that the copy number sensitivity of this locus could explain the gender differences in melanoma incidence and survival[34]. It is possible to speculate that despite its location in the pseudoautosomal region 1 (PAR1) of the X chromosome, sex may alter the effects of *PPP2R3B* expression in the germline as well. As our patients with duplications were however of both sexes, and the correlation between *PPP2R3B* expression and survival in the melanoma trancriptomic data was independent of sex, we do not currently have any evidence for such an effect.

Having discovered germline duplications in gene *PPP2R3B* in cohorts of individuals with melanocytic neoplasia, we sought to understand the mechanism of action. Our data demonstrate that *PPP2R3B* overexpression promotes proliferation of *NRAS*-mutant melanoma cell lines, which could explain the predisposition to the development of a clinically-apparent melanocytic naevus or melanoma in the context of a somatic pathogenic variant in a melanocyte. Alternatively, the pro-proliferative germline environment could in and of itself

predispose to somatic pathogenic variant in the skin, via increased cell division or alteration of cell cycle regulation and the associated effects on DNA repair. As we do not observe deletions in patient cohorts, only duplications, siRNA knockdown was not expected to produce biological effects. None of the CMN patients with duplications have so far developed melanoma, however this is in line with what would be expected statistically, as the incidence of melanoma in CMN at this age is very low[35], and no conclusions can yet be drawn about potential association between the *PPP2R3B* duplications and outcome in CMN. Interestingly, however, our data demonstrate clearly that increased *PPP2R3B* expression correlates with improved disease-specific survival in melanoma, mirroring the significant protective effect of *PPP2R3B* expression in urothelial cancer and pancreatic cancer datasets from the TCGA database[36]. A significant association between expression and survival is not seen in the smaller melanoma TCGA dataset, however this may be due to lack of statistical correction for known associated factors. In the larger melanoma cohort studied here, improved survival appears to be mediated via a non-immunological mechanism, and could potentially operate via phenotype switching towards proliferation and away from migratory potential (i.e. less metastatic potential).

Pigment cell phenotype switching is classically controlled by a reciprocal relationship between *MITF* and *POU3F2*[7,8,37,38], however we demonstrate clearly here that *PPP2R3B*-induced pigment cell phenotype switching is MITF-independent, and is instead driven by the relatively uncharacterised gene *C21orf91.* Although this mechanism could have involved the AKT/mTOR/pS6K pathway, signalling pathway alterations were largely unimpressive as measured by unbiased RPPA and by candidate immunoblotting, and indeed protein modelling

demonstrated a decrease in phosphatase activity with an increasing ratio of PR70 to the core enzyme.

We therefore hypothesised that if *PPP2R3B*-induced pigment cell phenotype switching was operating via *C21orf91*, perhaps MITF-induced proliferation also operates via *C21orf91*. This hypothesis is supported by the significant association between *MITF* and *C21orf91* expression in a melanoma cohort and pooled melanoma cell lines. Further supportive evidence for a role of *C21orf91* in this field includes its previous identification within a pro-proliferative anti-invasive transcriptomic signature in melanoma[39,40], a central role in cell phenotype determination in neurological development[41], and recognition as one of 180 key molecules in cross-species protein networks around the Ras-MAPK/PI3K pathways[42]. *MITF* knockdown in melanoma cells did indeed suppress *C21orf91* expression at baseline, and in a five-day real time proliferation assay *MITF* overexpression driving melanoma cell proliferation was rescued by knockdown of *C21orf91*.

The lack of positive association between *C21orf91* expression and *PPP2R3B* expression in the two transcriptomic datasets is potentially due to the multiple inputs to *C21orf91* as a hub, but could also be influenced by copy number changes to Xp which are relatively common in melanoma, affecting *PPP2R3B* expression.

Due to the highly repetitive nature of this region of the genome near the telomeric end of Xp, we found targeted NGS to be the most reliable way to detect and confirm duplications of *PPP2R3B*. Multiple custom-designed TaqMan® copy number assays (Thermo Fisher Scientific, USA) were insufficiently robust for diagnostic validation. Future screening of larger

melanoma cohorts and families will likely require development of a diagnostic-grade test from the point of view of cost, which will allow assessment of the frequency across different cohorts, of the penetrance of the melanoma phenotype associated with this variant, and association with clinical outcome.

We identify here germline duplications in the gene *PPP2R3B* predisposing to naevogenesis and melanoma in an important proportion of cases. Duplications increase melanocytic tissue expression of the protein product PR70, which confers a survival advantage in the context of melanoma, possibly via promotion of a pro-proliferative and anti-migratory pigment cell phenotype. This phenotype *in vitro* is driven by an undescribed MITF-independent mechanism mediated by *C21orf91*. This work offers novel insights into both the origins and behaviour of melanocytic neoplasia, and identifies *C21orf91* as an important new and potentially targetable fulcrum in the control of proliferation.

Ethical Approval

All participants gave written informed consent as part of ethically approved studies. The study of CMN genetics was approved by the London Bloomsbury Research Ethics Committee (REC) of Great Ormond Street Hospital (GOSH)/UCL Institute of Child Health (ICH). Samples from the Leeds Melanoma cohort was approved by the North East – _York Research ethics committee (Jarrow, Tyne and Wear, UK).

Data availability

Array CGH data have been submitted to http://www.ncbi.nlm.nih.gov/clinvar/. Melanoma transcriptomic data were deposited into the European Genome-phenome Archive (EGA) (accession no. EGAS00001002922 - https://ega-archive.org/studies/EGAS00001002922), access request to j.a.newton-bishop@leeds.ac.uk. Cell line *PPP2R3B* overexpression RNAseq data were deposited at the Gene Expression Omnibus (GEO) with accession number GSE145195, https://www.ncbi.nlm.nih.gov/geo/query/acc.cgi?acc=GSE145195, access request to veronica.kinsler@crick.ac.uk.

Conflict of interest

The authors declare no conflict of interest.

Acknowledgements

We gratefully acknowledge the participation of all patients. VAK, AT and the work presented in this study were funded by the Wellcome Trust (Grant WT104076MA). SP was funded by Caring Matters Now Charity and by the Newlife Foundation (Grant 15-16/10). The work was supported by the GOSHCC Livingstone Skin Research Centre, and by the UK National Institute for Health Research through the Biomedical Research Centre at Great Ormond St Hospital for Children NHS Foundation Trust, and the UCL GOS Institute of Child Health.

Author contributions

SP designed and carried out cellular modelling, RPPA, RNAseq, qRT-PCR and Western blot validations, proliferation and migration assays and immunocytochemistry, analysis of all associated data, produced the figures, and wrote the online methods. DZ designed and carried out MITF knockdown, overexpression and associated expression and proliferation studies. LA-O and ACT carried out MLPA copy number validation, the pilot NGS panel, RT-PCR tissue arrays, and analysis of data. DL designed and advised on the cellular modelling, RPPA, RNAseq and validations. MH, JN and JNB contributed patients and samples, with phenotypic, genotypic, and expression data and the associated analysis, and reviewed the manuscript. LH and GE analysed the NGS panel copy number data. SH and AP analysed the RNAseq, RPPA and regional similarity search data and produced the relevant figures. LH and GE analysed the NGS panel copy number data. NW, HC and YX designed and carried out the PR70 phosphatase activity and pull-down experiments, and reviewed the manuscript. PA, JM, VMdS, CC, GT, JAPB, and SP contributed patients, samples and phenotypic information. SB, RW and SMB conducted some sequencing experiments. DB and DM advised and helped analyse immunocytochemistry. PB was involved in early discussions of the genetic data. CH contributed patients and samples. Michael H advised on proliferation and migration assays. LL contributed cell line expression data and analysis with the relevant figure. SL and DH contributed to analysis of the array CGH data and validation. JM, SS, MZ contributed control cohort data on copy number. MM and WLD helped optimise cellular modelling and validation. KP and VB contributed patients and samples and reviewed the manuscript. NS analysed immunohistochemistry. Paulina S performed knock-down experiments and analysis. PS was involved in early discussion of the genetic data and reviewed the manuscript. EH and GM contributed to early research design and to the manuscript. JD helped conceive and direct the cellular modelling and signalling pathway characterisation, and contributed to the manuscript. VAK conceived, designed and directed the research, designed and carried out the initial human genetics experiments, contributed patients, analysed data, and wrote the manuscript.

CREdiT Statement

Conceptualization: VAK, EH, GM, JD

Formal Analysis: SP, VAK, LA-O, ACT, PS, AP, LL, LH, JNB, VAK, GE, NW, HC, YX ,SH, SL, SBM, DM, SL

Investigation: SP, DZ, DL, LA-O, ACT, PS, JN, MH, JNB, YX, LL, VAK

Methodology: SP, VAK, JD, DL, NW, HC, YX, MH, JN, JNB, DZ

Resources: PA, JM, VMdS, CC, GT, JAPB, DB, DM, CH, MM, WLD, KP AND VB, MH, JN, JNB, PS, RW, VAK, KP, JM SS, MZ, MH

Writing – original draft: VAK, JD, SP, EH, GM

Writing – review & editing: SP, EH, GM, PS, VAK

References

1. Harland M, Cust AE, Badenas C, et al. Prevalence and predictors of germline CDKN2A mutations for melanoma cases from Australia, Spain and the United Kingdom. Hered Cancer Clin Pract. 2014;12(1):20.
2. Kinsler VA, Thomas AC, Ishida M, et al. Multiple congenital melanocytic nevi and neurocutaneous melanosis are caused by postzygotic mutations in codon 61 of NRAS. The Journal of investigative dermatology. 2013;133(9):2229-2236.
3. Polubothu S, McGuire, N., Al-Olabi, L., Baird, W., Bulstrode, N., Chalker, J., Josifova, D., Lomas, D., Ong, J., Rampling, D., Sebire, N., Stadnik, P., Thomas, A., Wedgeworth, E., Kinsler, V.A. Genotype-phenotype-outcome cohort study of congenital melanocytic naevi – the relevance of genotype to clinical management. British Journal of Dermatology. 2018;in press.
4. Etchevers HC, Rose C, Kahle B, et al. Giant congenital melanocytic nevus with vascular malformation and epidermal cysts associated with a somatic activating mutation in BRAF. Pigment cell & melanoma research. 2018.
5. Kinsler VA, Birley J, Atherton DJ. Great Ormond Street Hospital for Children Registry for congenital melanocytic naevi: prospective study 1988-2007. Part 1-epidemiology, phenotype and outcomes. The British journal of dermatology. 2009;160(1):143-150.
6. Kinsler VA, Abu-Amero S, Budd P, et al. Germline melanocortin-1-receptor genotype is associated with severity of cutaneous phenotype in congenital melanocytic nevi: a role for MC1R in human fetal development. The Journal of investigative dermatology. 2012;132(8):2026-2032.
7. Goodall J, Carreira S, Denat L, et al. Brn-2 represses microphthalmia-associated transcription factor expression and marks a distinct subpopulation of microphthalmia-associated transcription factor-negative melanoma cells. Cancer research. 2008;68(19):7788-7794.
8. Hoek KS, Eichhoff OM, Schlegel NC, et al. In vivo switching of human melanoma cells between proliferative and invasive states. Cancer research. 2008;68(3):650-656.
9. Carreira S, Goodall J, Denat L, et al. Mitf regulation of Dia1 controls melanoma proliferation and invasiveness. Genes Dev. 2006;20(24):3426-3439.
10. MacDonald JR, Ziman R, Yuen RK, Feuk L, Scherer SW. The Database of Genomic Variants: a curated collection of structural variation in the human genome. Nucleic acids research. 2014;42(Database issue):D986-992.
11. Pang AW, Macdonald JR, Yuen RK, Hayes VM, Scherer SW. Performance of high-throughput sequencing for the discovery of genetic variation across the complete size spectrum. G3 (Bethesda). 2014;4(1):63-65.
12. 2019. https://www.mss.ng
13. RK CY, Merico D, Bookman M, et al. Whole genome sequencing resource identifies 18 new candidate genes for autism spectrum disorder. Nat Neurosci. 2017;20(4):602-611.
14. Bastian BC, Xiong J, Frieden IJ, et al. Genetic changes in neoplasms arising in congenital melanocytic nevi: differences between nodular proliferations and melanomas. The American journal of pathology. 2002;161(4):1163-1169.
15. Pozniak J, Nsengimana J, Laye JP, et al. Genetic and Environmental Determinants of Immune Response to Cutaneous Melanoma. Cancer research. 2019;79(10):2684-2696.

16. Yan Z, Fedorov SA, Mumby MC, Williams RS. PR48, a novel regulatory subunit of protein phosphatase 2A, interacts with Cdc6 and modulates DNA replication in human cells. Molecular and cellular biology. 2000;20(3):1021-1029.
17. Meyers RM, Bryan JG, McFarland JM, et al. Computational correction of copy number effect improves specificity of CRISPR-Cas9 essentiality screens in cancer cells. Nature genetics. 2017;49(12):1779-1784.
18. Broad D. DepMap Achilles 19Q1 Public. 2019.
19. Barretina J, Caponigro G, Stransky N, et al. The Cancer Cell Line Encyclopedia enables predictive modelling of anticancer drug sensitivity. Nature. 2012;483(7391):603-607.
20. Bak EJ, Choi KC, Jang S, et al. Licochalcone F alleviates glucose tolerance and chronic inflammation in diet-induced obese mice through Akt and p38 MAPK. Clinical nutrition. 2015.
21. Uhlen M, Fagerberg L, Hallstrom BM, et al. Proteomics. Tissue-based map of the human proteome. Science. 2015;347(6220):1260419.
22. Mace A, Kutalik Z, Valsesia A. Copy Number Variation. Methods in molecular biology. 2018;1793:231-258.
23. Monlong J, Cossette P, Meloche C, Rouleau G, Girard SL, Bourque G. Human copy number variants are enriched in regions of low mappability. Nucleic acids research. 2018;46(14):7236-7249.
24. Gerami P, Jewell SS, Morrison LE, et al. Fluorescence in situ hybridization (FISH) as an ancillary diagnostic tool in the diagnosis of melanoma. AmJSurgPathol. 2009;33(8):1146-1156.
25. Shi J, Zhou W, Zhu B, et al. Rare Germline Copy Number Variations and Disease Susceptibility in Familial Melanoma. The Journal of investigative dermatology. 2016;136(12):2436-2443.
26. Wlodarchak N, Xing Y. PP2A as a master regulator of the cell cycle. Crit Rev Biochem Mol Biol. 2016;51(3):162-184.
27. Eichhorn PJ, Creyghton MP, Bernards R. Protein phosphatase 2A regulatory subunits and cancer. BiochimBiophysActa. 2009;1795(1):1-15.
28. Cho US, Xu W. Crystal structure of a protein phosphatase 2A heterotrimeric holoenzyme. Nature. 2007;445(7123):53-57.
29. Janssens V, Goris J. Protein phosphatase 2A: a highly regulated family of serine/threonine phosphatases implicated in cell growth and signalling. BiochemJ. 2001;353(Pt 3):417-439.
30. Westermarck J. Targeted therapies don't work for a reason; the neglected tumor suppressor phosphatase PP2A strikes back. FEBS J. 2018;285(22):4139-4145.
31. Janssens V, Rebollo A. The role and therapeutic potential of Ser/Thr phosphatase PP2A in apoptotic signalling networks in human cancer cells. Curr Mol Med. 2012;12(3):268-287.
32. Baskaran R, Velmurugan BK. Protein phosphatase 2A as therapeutic targets in various disease models. Life Sci. 2018;210:40-46.
33. Mazhar S, Taylor SE, Sangodkar J, Narla G. Targeting PP2A in cancer: Combination therapies. Biochim Biophys Acta Mol Cell Res. 2019;1866(1):51-63.
34. van Kempen LC, Redpath M, Elchebly M, et al. The protein phosphatase 2A regulatory subunit PR70 is a gonosomal melanoma tumor suppressor gene. Science translational medicine. 2016;8(369):369ra177.

35. Kinsler VA, O'Hare P, Bulstrode N, et al. Melanoma in congenital melanocytic naevi. The British journal of dermatology. 2017;176(5):1131-1143.
36. TCGA database. 2019. http://cancergenome.nih.gov/.
37. Eisen T, Easty DJ, Bennett DC, Goding CR. The POU domain transcription factor Brn-2: elevated expression in malignant melanoma and regulation of melanocyte-specific gene expression. Oncogene. 1995;11(10):2157-2164.
38. Goodall J, Wellbrock C, Dexter TJ, Roberts K, Marais R, Goding CR. The Brn-2 transcription factor links activated BRAF to melanoma proliferation. Mol Cell Biol. 2004;24(7):2923-2931.
39. Verfaillie A, Imrichova H, Atak ZK, et al. Decoding the regulatory landscape of melanoma reveals TEADS as regulators of the invasive cell state. Nature communications. 2015;6:6683.
40. Ennen M, Keime C, Kobi D, et al. Single-cell gene expression signatures reveal melanoma cell heterogeneity. Oncogene. 2015;34(25):3251-3263.
41. Li SS, Qu Z, Haas M, et al. The HSA21 gene EURL/C21ORF91 controls neurogenesis within the cerebral cortex and is implicated in the pathogenesis of Down Syndrome. Sci Rep. 2016;6:29514.
42. Wang J, Yuan Y, Zhou Y, et al. Protein interaction data set highlighted with human Ras-MAPK/PI3K signaling pathways. J Proteome Res. 2008;7(9):3879-3889.
43. Vivas-García Y, Falletta P, Liebing J, et al. Lineage-Restricted Regulation of SCD and Fatty Acid Saturation by MITF Controls Melanoma Phenotypic Plasticity. Molecular cell. 2020;77(1):120-137.e129.

Figure legends

Figure 1.
Germline duplications involving PPP2R3B are found at increased frequency in individuals with melanocytic neoplasia
(a) Schematic of Xp22.33 demonstrating the location of three novel duplications (yellow) found in 24 CMN patients using whole genome array-CGH of leukocyte DNA, with one identical parental duplication demonstrating inheritance. Previously described copy number variants in that region are shown below, duplications in blue, deletions in red, with each bar representing a single publication. The publication representing a duplication involving *PPP2R3B* described a single variant in a cohort of approximately 36,000 (asterisk, and see text for details), confirming that the CMN duplications are rare in the normal population. (b) *PPP2R3B* duplications in a UK nonsyndromic melanoma cohort (4 duplications in non-selected cohort n=168), and CMN cohort (3 duplications in known pre-selected cohort n=5) shown by targeted next generation sequencing of *PPP2R3B*, in addition to the two telomeric genes (*GTPBP6* and *PLCXD1*) and the next centromeric gene (*SHOX*). Data represent the ratio of corrected read depth (see text for details) across the whole of *PPP2R3B* with respect to the ratio across the whole of *SHOX*. Each bar represents an individual patient. *PPP2R3B* duplications called are shown in light blue: validation of the array CGH findings in the three CMN patients are clustered to the right of the figure, and new duplications in the melanoma cohort in the rest of the figure (n=4, 2.4%).

Validation of PPP2R3B duplications detected by array CGH
Custom-designed MLPA® ratio plots validating copy number measurement of *PPP2R3B* (4 probes) and the two telomeric genes GTPBP6 and PLCXD1 (one probe each), to the left of each figure and less than 150bp in length; control probes of greater than 160kb targeting genes of known normal copy number across the genome are shown to the right at greater than 150bp size. A representative example of normal copy number for all genes (c), and of a duplication of *PPP2R3B* and *GTPBP6* and *PLCXD1* in a CMN patient (red dots) (d). While this method was able to validate the array CGH findings, it was not as robust as the targeted NGS panel for novel discovery of copy number changes, likely due to the repetitive, GC-rich, and polymorphic nature of the region studied.

Low-Copy Repeats at Xp22.33
(e) The upper panel depicts a regional similarity search across Xp22.33 with YASS software (http://bioinfo.cristal.univ-lille.fr/yass/index.php) both forwards (green) and backwards (red) revealing three segmental duplications (LCRA, LCRB and LCRC) 5' of *PPP2R3B* and a high density of SINE and LINE repeats. No segmental duplications are detected 3' to *PPP2R3B* before *SHOX*. The assembly gaps (red), local genes (purple) and the homology region (orange) with the Y chromosome are indicated.

Figure 2.

Germline duplications of *PPP2R3B* lead to increased expression of protein product PR70 in CMN tissue, compared to that of normal copy number controls.
(a, b) Immunohistochemical staining of formalin fixed paraffin embedded CMN tissue demonstrates moderate intensity PR70 staining throughout the cytoplasm of naevus cells in two patients where tissue was available with a confirmed germline *PPP2R3B* duplication and (c-f). negative PR70 staining in four patients with confirmed normal copy number of *PPP2R3B*. Stained sections were assessed by two independent blinded assessors and assigned a score of 1-3, based on the intensity of staining observed and scores averaged. Scores were: a=3, b=2.5, c=0, d=0, e=0 and f=0.

Increased *PPP2R3B* expression in melanoma tissue is correlated with improved melanoma specific survival.
(g) Kaplan-Meier curve generated from transcriptomic data from 703 FFPE melanoma tumours from the Leeds Melanoma Cohort, hazard ratio (HR) = 0.66, (95% confidence interval 0.50-0.88), p = 0.004. The effect remains significant after adjusting for age, sex, AJCC (American joint committee for cancer) stage, vascular invasion, site, *BRAF/NRAS* pathogen variant status and tumour invading lymphocytes (TILs). (h) Log intensity distribution of PPP2R3B DASL probe (ILMN_1689720) is close to a normal distribution.

Improved melanoma specific survival observed with increased expression of *PPP2R3B* appears not to be immune mediated.
Tumour expression of *PPP2R3B* correlates with expression of a large number of other genes in the genome: 596 positively correlated at FDR<0.05 with regression coefficient>0.20; 731 negatively correlated at FDR<0.05 with a regression coefficient<-0.2. (i) The genes positively correlated with *PPP2R3B* are predominantly enriched in non-immune pathways, consistent with the lack of association between *PPP2R3B* expression and TILs or any specific immune cell score. The genes negatively correlated with PPP2R3B expression are predominantly enriched in immune pathways (Table S1-2).

Figure 3.

Generation of stable inducible overexpression model for *PPP2R3B* in melanoma cell lines SKMEL2 and SKMEL30.

(a) Diagrammatic representation of stable inducible *PPP2R3B* overexpression system (SKMEL2-pTRIPZ-PPP2R3B and SKMEL30-pTRIPZ-PPP2R3B), and generation of samples for reverse phase protein arrays (RPPA) and RNA sequencing. Validation of *PPP2R3B* overexpression in samples for Reverse Phase Protein Array and RNAseq: (b) qRT-PCR demonstrating increased *PPP2R3B* mRNA in both induced cell lines at 6h and 16h hours (relative fold change in PPP2R3B expression, standardised to GAPDH, mean + SD of samples in quadruplicate), and, (c) Western blot confirming PR70 overexpression in induced cell lines at 6h and 16h hours with Vinculin loading control. Statistical significance was determined using a Student's t-test (Prism v7.0, Graphpad). Statistically significant values are indicated by a single asterisk ($p<0.05$), a double asterisk $p<0.01$, a triple asterisk ($p<0.001$) or a quadruple asterisk ($p<0.0001$). Overexpression of *PPP2R3B* increases proliferation in melanoma cell lines. (d), Increased proliferation following *PPP2R3B* overexpression using WST1 proliferation assay in SKMEL2-pTRIPZ-PPP2R3B at 6 hours, (e) in SKMEL30-pTRIPZ-PPP2R3B by BrdU assay at 24 hours (mean absorbance of colourmetric assay of eight replicates shown with standard deviation) and (f,g) by IncuCyte® cell count proliferation assay in SKMEL2-pTRIPZ-PPP2R3B and SKMEL30-pTRIPZPPP2R3B respectively over 100 hours, measuring confluence (%) versus time (hours) (mean confluence of eight replicates with standard deviation). (h, i) Mean confluence in each cell line is shown at timepoints of 50h and 100h respectively (mean of eight replicates standardised to non-induced cell line shown with standard error). Statistical analysis was performed and depicted as described above in figure legend. Overexpression of *PPP2R3B* decreases cellular migration in melanoma cell lines. (j,k) Scratchwound assay in SKMEL2-pTRIPZ-PPP2R3B and SKMEL30-pTRIPZ-PPP2R3B respectively leads to decreased relative wound confluence (%) versus time (hours) compared to noninduced controls. (l) Mean relative wound confluence in both cell lines shown at 48h (mean of eight replicates shown with error bars). Statistical analysis was performed and depicted as described above in figure legend.

Figure 4.

***PPP2R3B* overexpression affects mTOR/p70S6K1 and HIF-1 signalling pathways.**
(a,b) Heat map of protein expression observed by RPPA following overexpression of *PPP2R3B* in SKMEL2-pTRIPZ-PPP2R3B and SKMEL30-pTRIPZ-PPP2R3B respectively, demonstrating low background activity as expected from a controlled cellular model. (c,d) Volcano plots of log fold change in protein expression versus p-value for differentially expressed proteins common to both cell lines following *PPP2R3B* overexpression at 6h and 16h respectively. Unadjusted P-values < 0.05 are shown in red Raw data is available in supplementary material (Table S4).

PPP2R3B overexpression leads to significant and sustained rise in expression of gene *C21orf91*.
C21orf91 was the most differentially expressed gene on *PPP2R3B* induction common to both cell lines and at both time points by RNA sequencing (Table S5), other than *PPP2R3B* itself. (e) Heat map from pathway signature analysis of RNAseq data at 6h and 16h, focusing on pro proliferative anti-invasive melanoma signature genes38, demonstrating increased expression of *C21orf91* following *PPP2R3B* overexpression observed in both cell lines, at 6 and 16 hours. Validation of significantly increased *C21orf91* expression following *PPP2R3B* overexpression at 6h and 16h in both cell lines, shown by (f) qRT-PCR relative fold change in *C21orf91* mRNA levels, samples standardised to GAPDH (mean + SD of samples in quadruplicate) and (g,h) representative western blot with quantification of fold change of *C21orf91* - samples standardised to vinculin (mean shown with standard deviation of samples in triplicate). Statistical significance was determined using a Student's t-test (Prism v7.0, Graphpad). Statistically significant values are indicated by a single asterisk ($p<0.05$), a double asterisk $p<0.01$, a triple asterisk ($p<0.001$) or a quadruple asterisk ($p<0.0001$).

Figure 5.

Knockdown of *C21orf91* rescues increased proliferation associated with *PPP2R3B* overexpression.
IncuCyte® proliferation assay confluence (%) versus time (hours) for *PPP2R3B*-induced SKMEL2-pTRIPZ-PPP2R3B, with and without siRNA knock-down of *C21orf91* (a), with means taken at 100h (b) (mean confluence at given time point of eight replicates shown with standard deviation) shows a significant increase in proliferation following *PPP2R3B* induction, rescued by *C21orf91* knockdown and significantly different from knockdown with Scr siRNA. Statistical significance was determined using a Student's t-test (Prism v7.0, Graphpad). Statistically significant values are indicated by a single asterisk ($p<0.05$), a double asterisk $p<0.01$, a triple asterisk ($p<0.001$) or a quadruple asterisk ($p<0.0001$).

Knockdown of *C21orf91* rescues decreased migration associated with *PPP2R3B* overexpression.
IncuCyte® ScratchWound assay relative wound confluence (%) versus time (hours) for *PPP2R3B*-induced SKMEL2-pTRIPZ-PPP2R3B, with and without siRNA knock-down of *C21orf91* (c), with mean taken at 48h (d) (mean relative wound confluence at each time point of twelve replicates shown with standard deviation) shows a significant decrease in migration following *PPP2R3B* induction, rescued by *C21orf91* knockdown and significantly different from knockdown with Scr siRNA. Statistical significance was determined using a Student's t-test (Prism v7.0, Graphpad). Statistically significant values are indicated by a single asterisk ($p<0.05$), a double asterisk $p<0.01$, a triple asterisk ($p<0.001$) or a quadruple asterisk ($p<0.0001$).

Knockdown of *MITF* leads to decreased expression of *C21orf91*
qRT-PCR demonstrating decrease in both *MITF* and *C21orf91* mRNA following transfection by two different siRNAs targeting MITF transcript (siMITF 1 and siMITF 2) in SKMEL2 cell line (e). Relative fold change in gene expression compared to control cells transfected by non-target siRNA (siSCRA), standardised to GAPDH, mean + SD of 3 independent experiments.

Knockdown of *C21orf91* in cells rescues *MITF*-driven increase in proliferation
IncuCyte® proliferation assay confluence (%) versus time (hours) following overexpression of *MITF* in SKMEL2, with and without siRNA knock-down of *C21orf91* (f), with means taken at 100h (g) (mean confluence at given time point of four replicates shown with standard deviation). *MITF* overexpression drives proliferation as expected, which is rescued by knockdown of *C21orf91*. Controls for both transfection with the MITF overexpression vector and the C21orf91 siRNA are included. Statistical significance was determined using a Student's t-test (Prism v7.0, Graphpad). Statistically significant values are indicated by a single asterisk ($p<0.05$), a double asterisk $p<0.01$, a triple asterisk ($p<0.001$) or a quadruple asterisk ($p<0.0001$).

Increased expression of *C21orf91* is associated with genetic dependency on MITF in melanoma cell lines
(h) CRISPR-Cas9 genome-scale knockout of MITF in melanoma cell lines (n=30) reveals increased expression of *C21orf91* in cells with greater MITF dependency, suggesting that C21orf91 is downstream of MITF. Dependency score as described in https://depmap.org.

PR70 and C21orf91 are expressed throughout the cytoplasm with increased expression of C21orf91 in dividing cells

(i) Immunocytochemistry of SKMEL30-pTRIPZ-PPP2R3B in uninduced cells at 10X (A) and induced cells at 10X (B) and 20X (C) confirms increased PR70 and C21orf91 expression throughout the cytoplasm following induction of *PPP2R3B*. PR70 is stained with Alex Fluor® 488 (green) secondary antibody, and nuclei stained with Hoescht (blue) and in (C) Phalloidin (actin) is visualised with a conjugated Alex Fluor® 647 (far red) antibody. C21orf91 expression is increased in cells with two nuclei, which could be due to various causes including cell division or a cytokinesis defect 10X (D), 20X (E), 40X (F), stained with Alexa Fluor® 488 (green) secondary antibody, and Hoescht nuclear stain (blue). Scale bars represent 100 microns.

RE:

Inherited duplications of *PPP2R3B* promote naevi and melanoma via a novel *C21orf91*-driven proliferative phenotype

Corresponding author

Veronica Kinsler, The Francis Crick Institute, 1 Midland Rd, London NW1 1AT; veronica.kinsler@crick.ac.uk

Conflict of interest statement

The authors declare no conflict of interest.

Figure 1

Figure 2

Click here to access/download

Figure

Post acceptance Figure 2 April 2021.pdf

Figure 3

Click here to access/download

Figure

Post acceptance Figure 3 April 2021.pdf

Figure 4

Click here to access/download

Figure

Post acceptance Figure 4 April 2021.pdf

Figure 5

Click here to access/download

Figure

Post acceptance Figure 5 April 2021.pdf

Supplementary Materials

Materials and Methods

Patient recruitment and approvals

All participants gave written informed consent as part of ethically approved studies. CMN patients were recruited from Great Ormond Street Hospital (GOSH) London, with London Bloomsbury Research Ethics Committee (REC) approval, and melanoma samples were obtained from Professor Newton-Bishop, Leeds, with approval from North East – York UK REC. DNA was extracted from blood samples using standard methods in all cohorts.

Sample preparation for Reverse Phase Protein Array and RNAseq

SKMEL30 pTRIPZ-PPP2R3B and SKMEL2 pTRIPZ-PPP2R3B cells were seeded and induced with doxycycline 1µg/ml for either 6 hours or 16 hours alongside untreated controls. Samples were collected in triplicate for both RNA extraction and protein lysis. Confirmation of *PPP2R3B* induction was performed by qPCR and Western blotting.

Immunohistochemistry

PR70 expression was assessed using an optimised protocol with antibody against PR70 (Key Resources - Table S1). FFPE sections were dewaxed, rehydrated and heat mediated antigen retrieval was performed. Sections were blocked for one hour at room temperature in 1% FBS 10% BSA prior to incubation in primary antibody in blocking solution at 1:50 overnight at 4°C. Sections were incubated with HRP-tagged secondary antibody at 1:500 for one hour at room temperature. Samples were treated with hydrogen peroxide 0.3% for 10 minutes at room temperature prior to application of DAB chromogen for 6 minutes, following which sections were dehydrated and mounted. Between steps sections were washed three times for 5 minutes in PBS Tween 0.05%. Slides were scanned using a Zeiss Axio Scan.X1 slidescanner at 20X. Staining was graded in naevus nests as 0-3 intensity of DAB staining by two blinded assessors (SP, VK).

Quantitative Real Time PCR

1µg of total RNA was reverse transcribed and quantitative real time PCR performed, using Taqman probes (Key Resources - Table 2) and the StepOnePlus Real-Time PCR System (ABI, Abilene, TX, USA). Relative fold change to the housekeeping gene *GAPDH* was calculated by the $\Delta\Delta$CT method.

Western Blotting

Protein lysate was quantified by Bradford protein assay, and 20ug of each sample run on a 10% Bis-Tris protein gel. PVDF membrane was activated in methanol prior to wet transfer. The membrane was washed three times in TBST, then blocked using 3% albumin at room temperature for one hour. Membranes were then incubated in primary antibody (**Table S1**) in 3% albumin overnight at 4°C. Membranes were washed three times in TBST then incubated in corresponding HRP-tagged secondary antibody in 5% milk for 1 hour at room temperature. Membranes were washed a further three times in TBST before adding ECL for two minutes followed by measurement of chemiluminescence using Amersham Imager 600. Intensity of bands was quantified using ImageJ software.

Immunocytochemistry

4 x 10^4 cells were seeded per well in laminin-coated 4-well chamber slides (Millicell® EZ slide, Merck Millipore, PEZGS0816), washed in cold PBS and fixed using 4% paraformaldehyde (PFA), followed by permeabilisation using 0.1% Triton X100. After three washes with PBS they were incubated with blocking solution (1% Bovine serum albumin, 10% Donkey serum, 0.3M Glycine, 0.1% PBS Tween) for 1 hour at room temperature followed by primary antibody (**Table S1**) in blocking solution overnight at 4°C. Slides were washed once with 1:10,000 Hoechst, three times with 0.1% PBS Tween, and incubated with appropriate fluorescent secondaries at room temperature for one hour in the dark. Slides were again washed three times with 0.1% PBS Tween and mounted prior to analysis.

MLPA®

Customised MLPA® was performed as per MRC-Holland MLPA® DNA protocol version MDP-v003, optimized using 25ng of DNA per well, and a 1 in 2 dilution of the customised probemix, using four probes for *PPP2R3B,* and one each for *GTPBP6* and *PLCXD1* designed to dovetail by

size with the pan-genome probes of known normal copy number in the reference SALSA® MLPA® probemix P200-A1 (MRC-Holland). Capillary electrophoresis of diluted PCR products with ROX-500 size standard was performed on an ABI 3730xl, and data analysed using GeneMarker® v2.4 (SoftGenetics, USA). Each plate contained the same controls of normal copy number and duplication for standardisation. A duplication was determined if all four probes within PPP were at a ratio of 1.3:1 or higher, whilst all the control probes were at 1:1 ratio.

Validation of antibodies by CRISPR/Cas9 knockout

Antibodies for PR70 (*PPP2R3B* - Abcam ab234731) and C21orf91 (Sigma HPA049030 and Abcam ab80695) were validated using CRISPR/Cas9 knockout of the genes in question in the HEK293 cell line. CRISPR/Cas9 knockouts were generated using the Alt-R CRISP-Cas9 system (Integrated DNA Technologies). Briefly, three guide RNAs per gene were designed and produced as crRNAs (see Key resources - Table 3). Duplex guide RNAs were produced following incubation of each crRNA with a fluorescently labelled tracerRNA at 95°C, which were then complexed with Cas9 protein to form a ribonucleoprotein (RNP) transfection complex. Reverse transfection of three different RNP complexes plus a pooled RNP complex for each of the two genes was achieved using CRISPRMAX™ (Thermofisher, Invitrogen), and addition of 50µl of RNP complex (final concentration of both guide RNA and Cas9 60nM) to 8 x 10^5 HEK cells in one well of a 6 well plate. Cells were incubated at 37°C, 5% CO_2 for 24 hours prior to single cell sorting by flow cytometry of the population of cells containing the fluorescent tracerRNA into a 96 well plate. Single cell colonies were expanded to 6 well plates and DNA extracted using QuickExtract DNA extraction solution (Lucigen) and protein lysate harvested by standard methods. Sanger sequencing confirming frameshift indels, and immunoblotting for each protein product in the presence of control cell lines confirmed complete protein absence **(Figure S5)** and therefore target specificity of each antibody.

***PPP2R3B* knockdown IncuCyte® Cell Count Proliferation Assay**

SKMEL2 cells were seeded into a 96 well ImageLock plate at a density of 1 x 10^4 cells per well. *PPP2R3B* knockdown was achieved in selected cells by transefction with Lipofectamine™ RNAiMAX using a pooled *PPP2R3B* siRNA (ON-TARGETplus Human *PPP2R3B*, Dharmacon 28227) at 10nM alongside mock and scrambled siRNA transfections. Efficacy of knockdown

at mRNA level was confirmed at concentrations of 10nM and 25nM by qRT-PCR (Figure S6a). The plate was then analysed using the IncuCyte® live-cell analysis system and set up to acquire 10X phase contrast images at a scanning interval of 60 minutes for 5 days, measuring percentage confluence. Confluence was averaged between 12 replicates for each condition (mean + SD) and statistical significance was calculated by Students t-test **(Figure S6b-d)**.

Protein preparation, and holoenzyme assembly with PR70 and B'γ1 regulatory subunits via GST-mediated pull-down assay

Expression and purification of PP2A Aα (9-589), Cα (1-309), PR70 subunit, and Cdc6, and assembly of the PP2A core enzyme (Aα-Cα heterodimer) followed procedures described previously. Approximately 10 μg of GST-AC (core enzyme) was bound to 10μl of glutathione resin via GST tag. The resin was washed with 200μl assay buffer three times to remove the excess unbound protein. Then, the indicated amounts of PR70 and B'γ1 were added to the resin in a 200μl volume suspended in the assay buffer containing 25 mM Tris (pH 8.0), 150 mM NaCl, 1 mM $CaCl_2$, and 3 mM DTT. The mixture was washed three times with the assay buffer. The proteins remained bound to resin were examined by SDS-PAGE, and visualized by Coomassie blue staining. All experiments were repeated three times. The level of binding was quantified using Image J, and results from three separate experiments were fitted in GraphPad Prism (GraphPad Software, Inc.).

Phosphatase assay

Purified GST-Cdc6 (49-90) was phosphorylated *in vitro* by Cyclin A/CDK2 (1/20 w/w) with 10 mM $MgCl_2$ and 10x molar concentration of ATP for 1 hour at 30^{o}C. The phosphorylated protein was purified by gel filtration chromatography (Superdex 200, GE Healthcare) to remove free ATP, followed by overnight cleavage of the GST-tag with TEV protease (1/20 w/w). The pCdc6 peptide was then separated from GST or uncleaved peptide using untrafiltration membrane (Millipore) with a 10 kDa cut-off. The phosphatase assay was performed in 100μl assay volume (rather than 50 μL) at room temperature for 15 minutes and stopped by the addition of 2x malachite green (50 μL) rather than 100 μL of 1x malachite green to increase the sensitivity of the assay. The phosphatase activity of 0.16 μM of PP2A

core enzyme was measured using 2.2 μM pCdc6 peptide in a buffer containing 25 mM Tris pH 8.0, 150 mM NaCl, 3mM DTT, 50 μM $MnCl_2$ and 1 mM $CaCl_2$, in the presence and absence of the indicated concentrations of PR70 (108-519). The absorbance at 620 nm was measured after 10 min incubation at room temperature. The PR70 concentration-dependent PP2A phosphatase activity toward pCdc6 was fitted in GraphPad Prism (GraphPad Software, Inc.) by two separate simulations for two ranges of PR70 concentrations, lower versus higher than the molar concentration of PP2A core enzyme. The experiments were repeated three times, representative results were shown.

Mammalian cell culture, recombinant expression of PR70, and fractionation of cell lysate via gel filtration chromatography followed by western blot

293T and C6 glioma cells were cultured in Dulbecco's modified Eagle's medium (DMEM) supplemented with 10% fetal bovine serum (FBS), 100 units/ml of penicillin, and 100 μg/ml of streptomycin. The V5-tagged human PR70 (V5-PR70) was cloned into murine leukemia retroviral vectors harboring a CMV promoter for over-expression. Retroviruses harboring V5-PR70 were packaged in 293T cells, and were used to infect 293T or C6 glioma cells with 50-80% confluence for over-expression of V5-PR70. The infection efficiency of retroviruses was monitored by the fluorescence signals of RFP or GFP included in retroviral vectors. The level of recombinant V5-PR70 in holoenzyme versus as free subunit were determined by fractionation of cell lysate over gel filtration chromatography to examine co-migration of V5-PR70 with the scaffold A and PP2Ac subunits. The relative amounts of A, PP2Ac, and V5-PR70 in each fraction were determined by western blot using antibodies that specifically recognize A (Millipore), PP2A Cα subunit (Millipore, 1D6), and V5-tag (Millipore), followed by quantification of the western blot signals using Image J. The experiment was repeated three times; representative results are shown.

Key Resources

Supplemental Table 1 - Antibodies:

Antibody	Source	Catalogue Number	Dilution
PPP2R3B	Rabbit	Abcam, ab72027	1:1000 Western Blot 1:500 Immunocytochemistry
MITF	Mouse	Abcam ab3201	1:1000
Vinculin	Mouse	Cell signaling technology #4650S	1:1000
C21orf91	Rabbit	Altas Antibodies, HPA018288	1:1000 Western Blot 1:500 Immunocytochemistry
MYC-tag	Mouse	Abcam ab32	1:2000 Western Blot 1:500 Immunocytochemistry
S6K1	Rabbit	Abcam ab32529	1:1000
AKT	Rabbit	Cell signaling technology #4685	1:1000
Phospho AKT S473	Rabbit	Cell signaling technology #9271	1:1000
Phospho AKT T308	Rabbit	Cell signaling technology #13038	1:1000
MYC	Mouse	Abcam ab32072	1:1000

Supplemental Table 2 - Taqman® probes:

TaqMan® Probe 20X	Source, Catalogue Number
PPP2R3B	Hs00203045_m1
C21orf91	Hs00213743_m1
GAPDH	Hs02786624_g1
MITF	Hs01117294_m1

Figure S1.

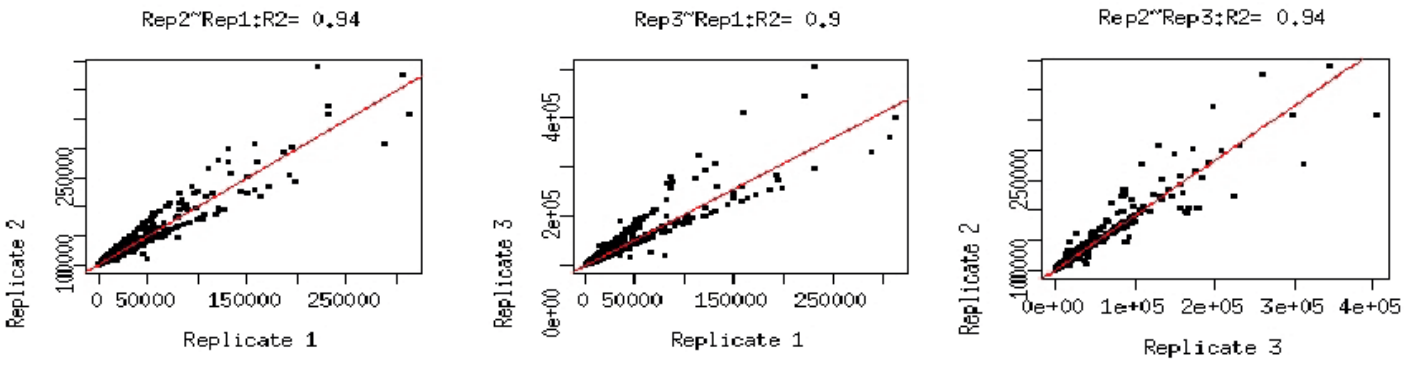

Figure S2.

a)

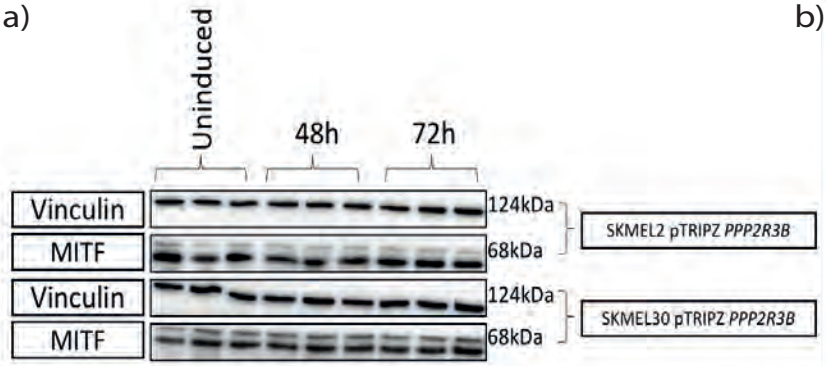

b)

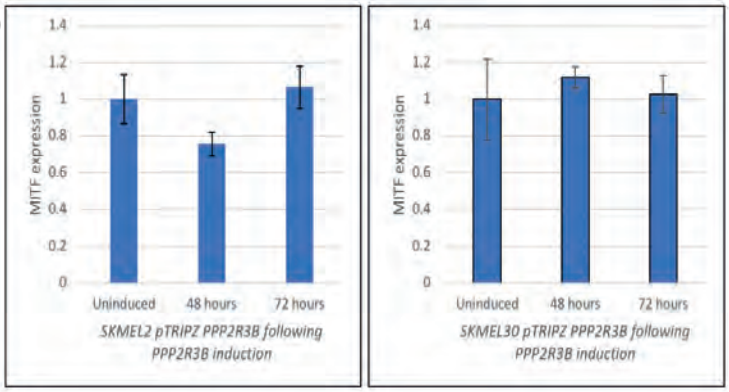

Figure S1

Replicates of induced and uninduced cells used in RNAseq show good correlation. From left to right, correlation between 1st and 2nd replicates, 1st and 3rd replicates and 2nd and replicates.

Figure S2

Overexpression of *PPP2R3B* does not induce proliferation via MITF. Western blot of uninduced and induced SKMEL2 pTRIPZ *PPP2R3B* and SKMEL30 pTRIPZ *PPP2R3B* cells for MITF expression **(a),** and quantification **(b),** show *PPP2R3B* overexpression does not consistently alter MITF activation across the cell lines in this system, suggesting the increased proliferation in cell lines observed following *PPP2R3B* overexpression is MITF independent

Figure S3.

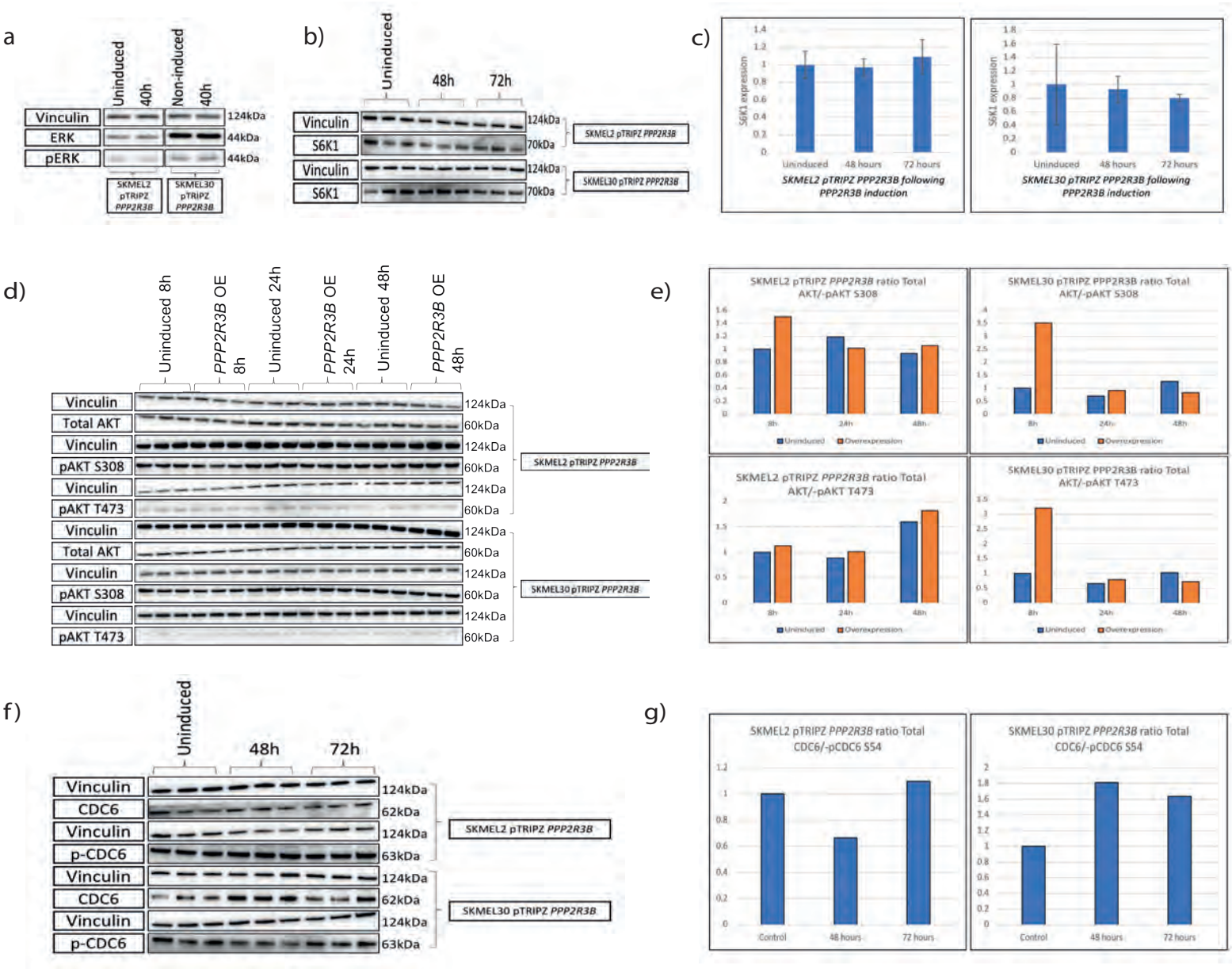
a
Uninduced
40h
Non-induced
40h
Vinculin
ERK
pERK
124kDa
44kDa
44kDa
SKMEL2 pTRIPZ PPP2R3B
SKMEL30 pTRIPZ PPP2R3B
b)
Uninduced
48h
72h
Vinculin
S6K1
Vinculin
S6K1
124kDa
70kDa
124kDa
70kDa
SKMEL2 pTRIPZ PPP2R3B
SKMEL30 pTRIPZ PPP2R3B
c)
S6K1 expression
Uninduced
48 hours
72 hours
SKMEL2 pTRIPZ PPP2R3B following PPP2R3B induction
S6K1 expression
Uninduced
48 hours
72 hours
SKMEL30 pTRIPZ PPP2R3B following PPP2R3B induction
d)
Uninduced 8h
PPP2R3B OE 8h
Uninduced 24h
PPP2R3B OE 24h
Uninduced 48h
PPP2R3B OE 48h
Vinculin
Total AKT
Vinculin
pAKT S308
Vinculin
pAKT T473
Vinculin
Total AKT
Vinculin
pAKT S308
Vinculin
pAKT T473
124kDa
60kDa
124kDa
60kDa
124kDa
60kDa
124kDa
60kDa
124kDa
60kDa
SKMEL2 pTRIPZ PPP2R3B
SKMEL30 pTRIPZ PPP2R3B
e)
SKMEL2 pTRIPZ PPP2R3B ratio Total AKT/-pAKT S308
SKMEL30 pTRIPZ PPP2R3B ratio Total AKT/-pAKT S308
SKMEL2 pTRIPZ PPP2R3B ratio Total AKT/-pAKT T473
SKMEL30 pTRIPZ PPP2R3B ratio Total AKT/-pAKT T473
8h
24h
48h
Uninduced
Overexpression
f)
Uninduced
48h
72h
Vinculin
CDC6
Vinculin
p-CDC6
Vinculin
CDC6
Vinculin
p-CDC6
124kDa
62kDa
124kDa
63kDa
124kDa
62kDa
124kDa
63kDa
SKMEL2 pTRIPZ PPP2R3B
SKMEL30 pTRIPZ PPP2R3B
g)
SKMEL2 pTRIPZ PPP2R3B ratio Total CDC6/-pCDC6 S54
SKMEL30 pTRIPZ PPP2R3B ratio Total CDC6/-pCDC6 S54
Control
48 hours
72 hours

Figure S3

Overexpression of *PPP2R3B* dephosphorylates AKT, but does not consistently affect CDC6 activation.

Western blots of lysate from uninduced and induced SKMEL2-pTRIPZ-PPP2R3B and SKMEL30-pTRIPZ-PPP2R3B cells, for (a) ERK and phospho-ERK, (b,c) S6K1 with quantification, (d,e) AKT and phospho-AKT (S308 and T473) with quantification of ratio of total to phospho-AKT, demonstrate *PPP2R3B* overexpression decreases phosphorylation of AKT at 6-8 hours, but does not lead to strong activation of known melanoma signalling pathways. Western blots of (f,g) CDC6 and phospo-CDC6 and quantification of ratio of total to phospho-CDC6, show *PPP2R3B* overexpression does not consistently alter CDC6 activation across the cell lines in this system. This is supported by direct phosphatase activity measurements in another cellular model demonstrating that the interaction between PR70 and CDC6 may be dose-dependent (Figure S4).

Figure S4.

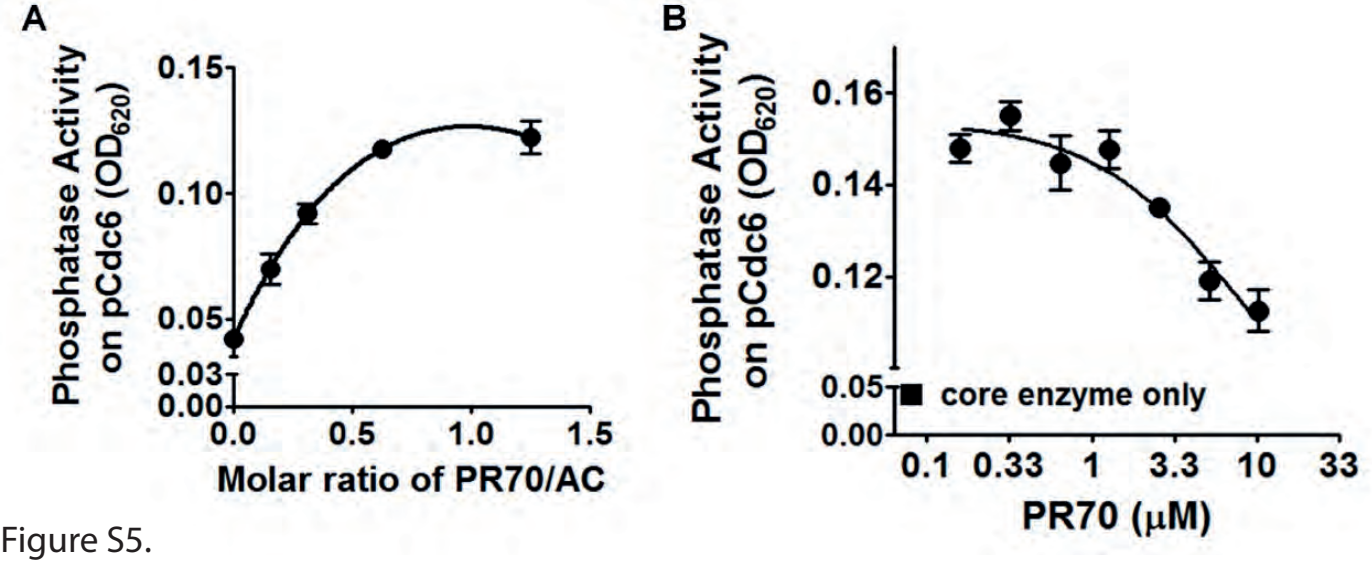

Figure S5.

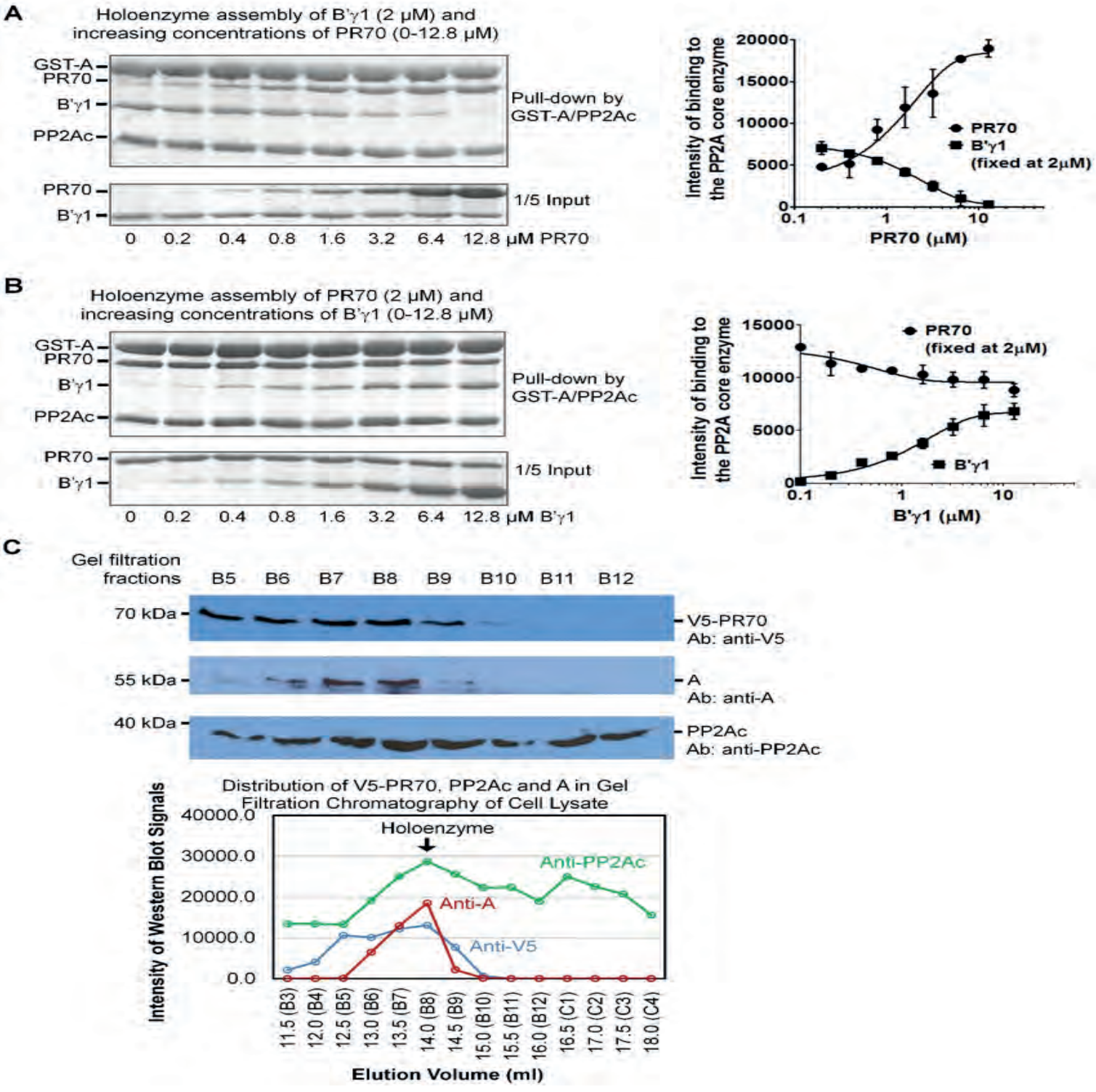

Figure S4

Increasing concentrations of PR70 gave increased PP2A activity toward its specific substrate, pCdc6, a cell cycle regulator that participates in tight control of replication licensing[41] **(a)**. However, when the molar concentration of PR70 was higher than PP2A core enzyme, further increase of PR70 level reduced the phosphatase activity of PP2A, possibly due to a dominant negative effect via competitive inhibition **(b)**.

Figure S5

PR70 efficiently competes with the B'γ1 regulatory subunit for holoenzyme assembly

A). Pull-down of a fixed concentration of B'γ1 in the presence and absence of increasing concentrations of PR70 via GST-tagged PP2A core enzyme (A/PP2Ac). The bound proteins were visualized on SDS-PAGE by Coomassie blue staining. PR70 efficiently reduced the holoenzyme assembly with the B'γ1 regulatory subunit. B). Pull-down of a fixed concentration of PR70 in the presence and absence of increasing concentrations of B'γ1 similar to that described in A). B'γ1 could barely compete with PR70 for holoenzyme assembly. For both panel A) and B), the experiments were repeated three times; representative results are shown. The simulation of the quantified data from three repeats was shown on the right. C). Western blot detection of A, PP2Ac, and recombinant V5-PR70 in fractions of gel filtration chromatography of cell lysates with overexpressed V5-PR70. The distribution curves of the three components are shown in the lower panel.

Figure S6.

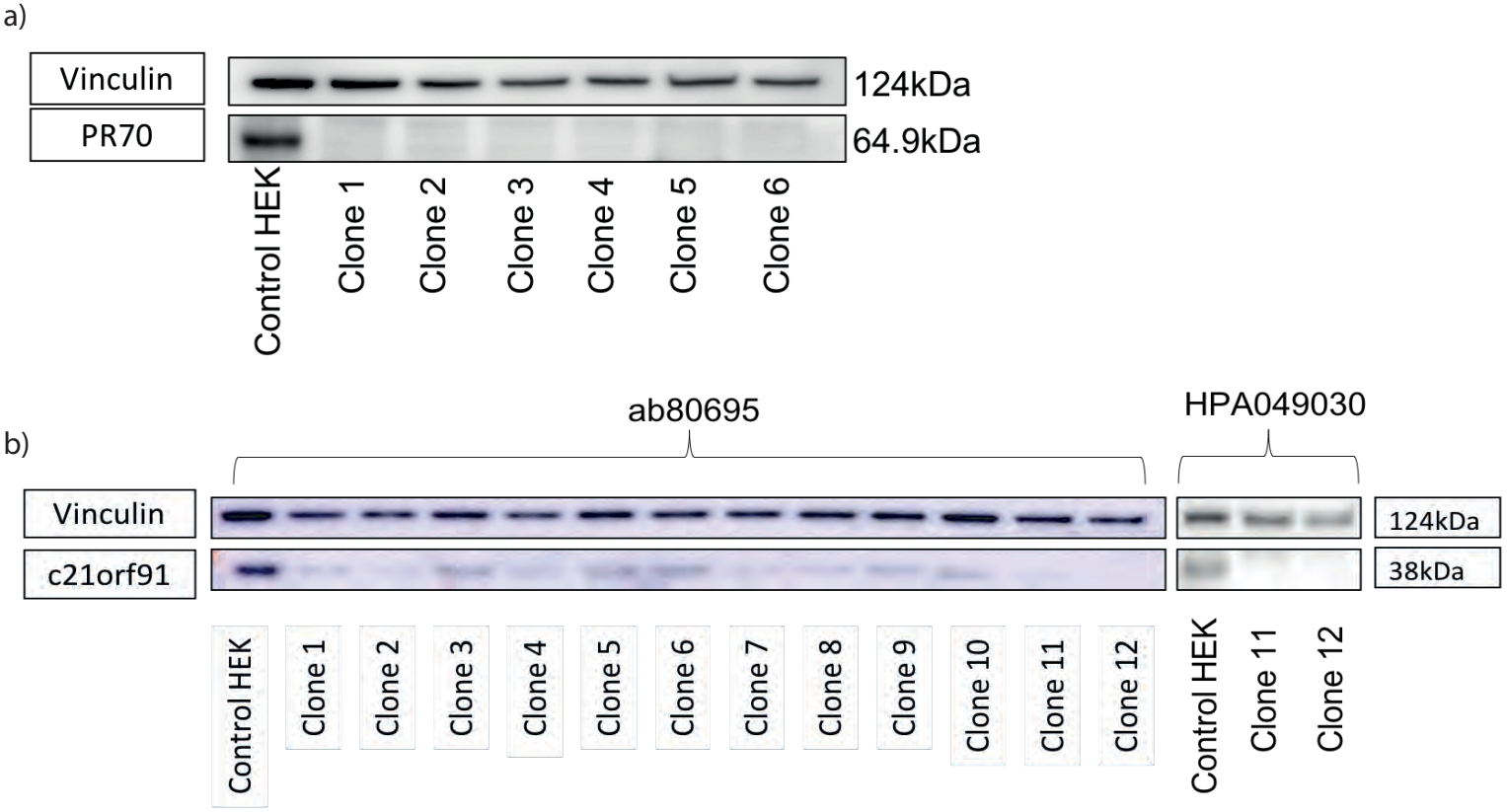
a)
Vinculin
PR70
124kDa
64.9kDa
Control HEK
Clone 1
Clone 2
Clone 3
Clone 4
Clone 5
Clone 6
b)
ab80695
HPA049030
Vinculin
c21orf91
124kDa
38kDa
Control HEK
Clone 1
Clone 2
Clone 3
Clone 4
Clone 5
Clone 6
Clone 7
Clone 8
Clone 9
Clone 10
Clone 11
Clone 12
Control HEK
Clone 11
Clone 12

Figure S6

Validation of PR70 antibody (Abcam ab234731) and C21orf91 antibodies (Sigma, HPA049030 and Abcam ab80695) using CRISPR-Cas9 knockout cell lines

Western blot of a) PPP2R3B CRISPR-Cas9 HEK293 single cell clones demonstrates no expression of PR70 in comparison to control protein lysate from HEK293 and b) C21orf91 CRISPR-Cas9 HEK293 single cell clones demonstrates no expression of C21orf91 in knockout clones 11 and 12 using both C21orf91 antibodies in comparison to control protein lysate from HEK293. Corresponding Sanger sequencing from knockout cell lines confirms knockout.

Figure S7.

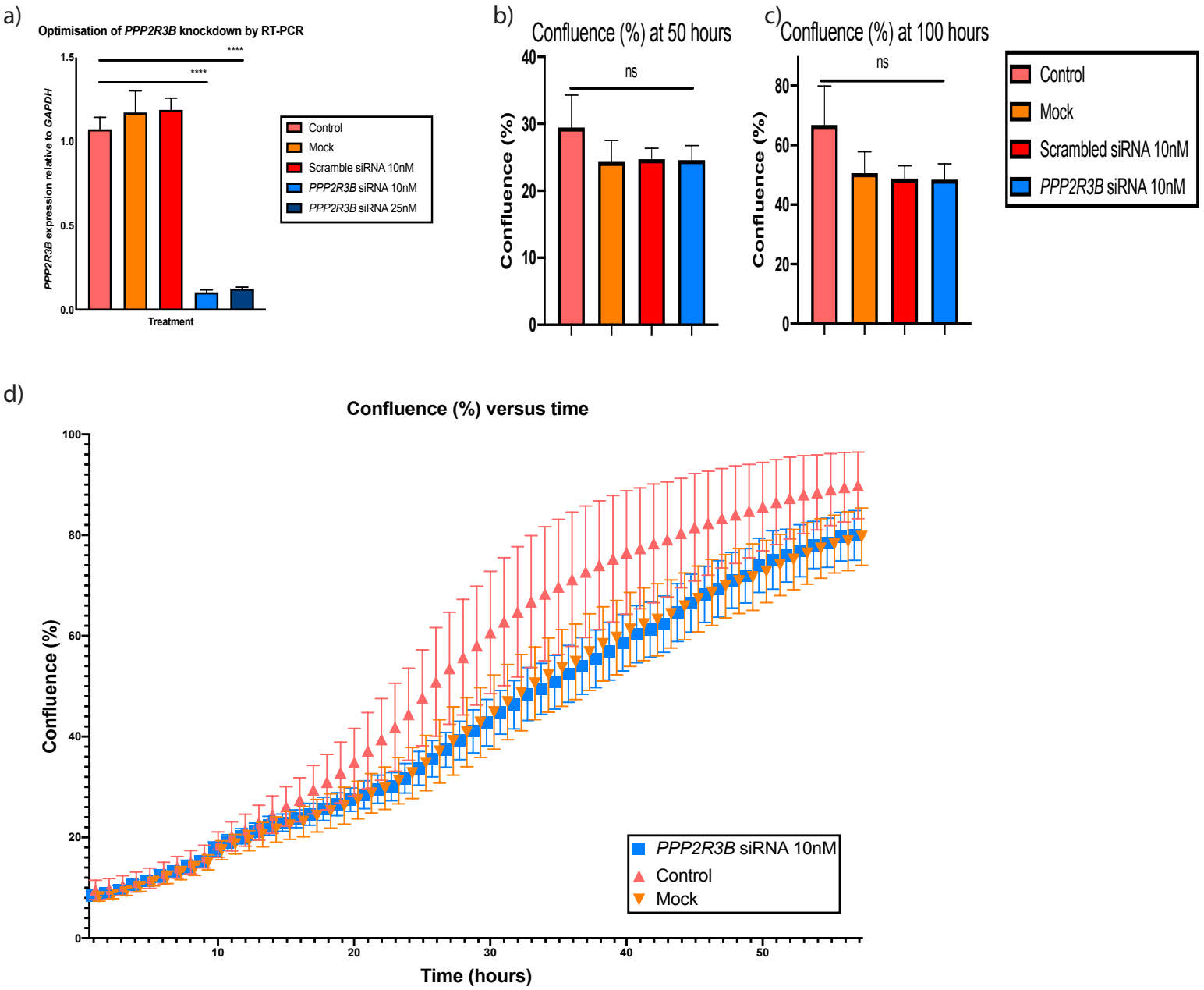
a)
Optimisation of PPP2R3B knockdown by RT-PCR
PPP2R3B expression relative to GAPDH
Treatment
****
****
Control
Mock
Scramble siRNA 10nM
PPP2R3B siRNA 10nM
PPP2R3B siRNA 25nM
b)
Confluence (%) at 50 hours
Confluence (%)
ns
c)
Confluence (%) at 100 hours
Confluence (%)
ns
Control
Mock
Scrambled siRNA 10nM
PPP2R3B siRNA 10nM
d)
Confluence (%) versus time
Confluence (%)
Time (hours)
PPP2R3B siRNA 10nM
Control
Mock

Figure S7

***PPP2R3B* knockdown is not shown to have a significant effect on proliferation in SKMEL2**

Validation of PPP2R3B knockdown in SKMEL2 demonstrates efficient knockdown of PPP2R3B at RNA level at siRNA concentrations of 10nM and 25nM in comparison to control, mock and scrambled siRNA 10nM by RT-PCR **(a).** Mean expression of four replicates is shown with standard deviation. Statistical significance was determined using a Student's t-tests. No significant effect on proliferation is observed following *PPP2R3B* knockdown in SKMEL2 using IncuCyte® cell count proliferation assay over 100 hours, measuring confluence (%) versus time (hours) in comparison to control, mock and scrambled siRNA 10nM **(b)** (mean confluence at each time point of eight replicates shown with standard deviation). The mean confluence with standard deviation is shown at timepoints of 50h **(c)** and 100h **(d).** Statistical significance was determined using a Student's t-tests at each time point.

Figure S8.

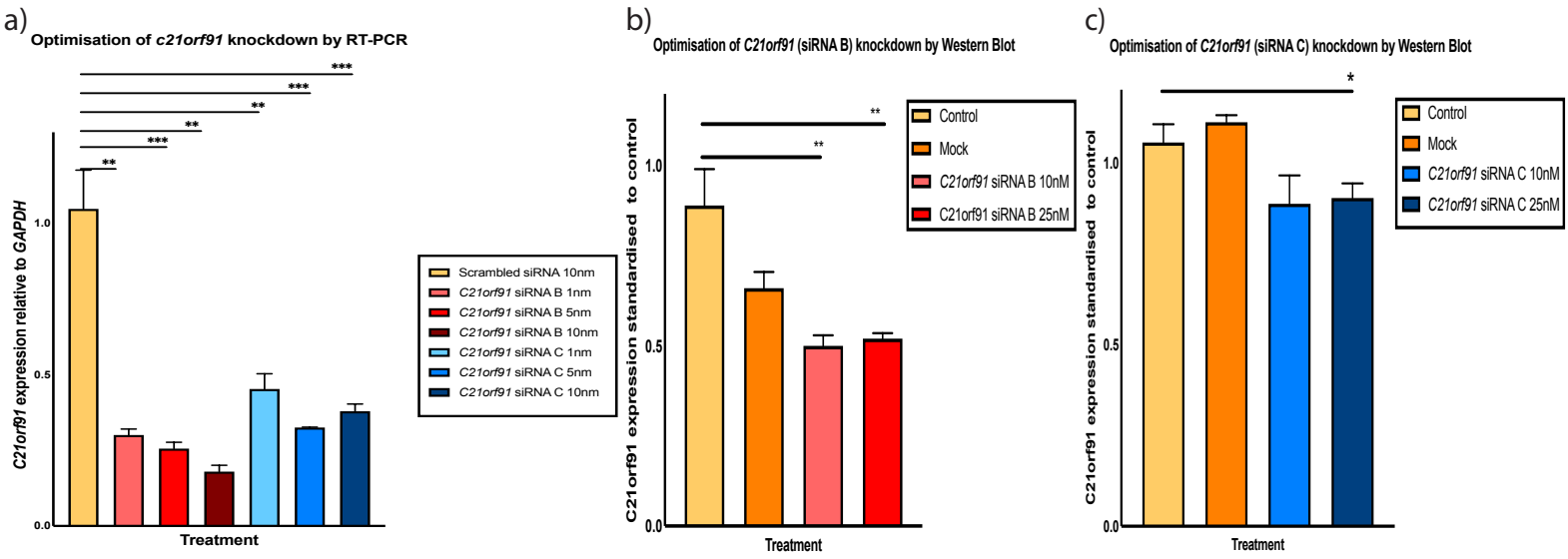
a)
Optimisation of c21orf91 knockdown by RT-PCR
C21orf91 expression relative to GAPDH
Treatment
Scrambled siRNA 10nm
C21orf91 siRNA B 1nm
C21orf91 siRNA B 5nm
C21orf91 siRNA B 10nm
C21orf91 siRNA C 1nm
C21orf91 siRNA C 5nm
C21orf91 siRNA C 10nm
b)
Optimisation of C21orf91 (siRNA B) knockdown by Western Blot
C21orf91 expression standardised to control
Treatment
Control
Mock
C21orf91 siRNA B 10nM
C21orf91 siRNA B 25nM
c)
Optimisation of C21orf91 (siRNA C) knockdown by Western Blot
C21orf91 expression standardised to control
Treatment
Control
Mock
C21orf91 siRNA C 10nM
C21orf91 siRNA C 25nM

Figure S8

Validation of *C21orf91* knockdown in SKMEL2

Validation of *C21orf91* knockdown in SKMEL2 demonstrates efficient knockdown of two *C21orf91* siRNAs at RNA level at concentrations of 1nM, 5nM and 10nM in comparison to scrambled siRNA 10nM by RT-PCR **(a).** Mean expression of four replicates is shown with standard deviation. Statistical significance was determined using a Student's t-tests. C21orf91 knockdown demonstrated at protein level by Western blot using two *C21orf91* siRNAs 10nM in comparison to control and mock transfection, siRNA B **(b)** and siRNA c **(c)**. Mean expression of three replicates is shown with standard deviation. Statistical significance was determined using a Student's t-tests.

Figure S9.

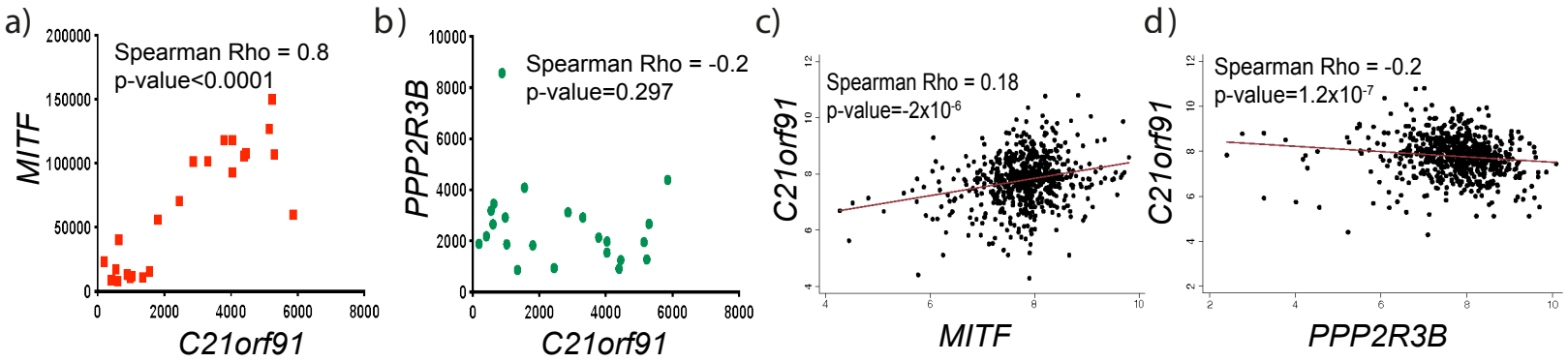
a)
Spearman Rho = 0.8
p-value<0.0001
MITF
C21orf91
b)
Spearman Rho = -0.2
p-value=0.297
PPP2R3B
C21orf91
c)
Spearman Rho = 0.18
p-value=-2x10-6
C21orf91
MITF
d)
Spearman Rho = -0.2
p-value=1.2x10-7
C21orf91
PPP2R3B

Figure S9

C21orf91 and MITF expression are significantly positively correlated in melanoma, independent of PPP2R3B.

(a) Positive correlation observed between expression of between expression of *C21orf91* and *MITF* demonstrated in independent transcriptomic data from a cohort of 24 human derived melanoma cell lines, Spearman Rho 0.8 (95% CI 0.6-0.9, p<0.0001), but (b) no correlation observed between expression of *C21orf91* and *PPP2R3B*. Similarly, (c) positive correlation demonstrated in independent transcriptomic data in human melanoma tissue Spearman Rho 0.18 ($p = 2 \times 10^{-6}$) but (d) negative correlation observed between expression of *C21orf91* and *PPP2R3B,* Spearman Rho -0.2 ($p = 1.2 \times 10^{-7}$). This points to increased expression of *C21orf91* as a new hub in melanocytic proliferation, not only a target of *PPP2R3B*. Increased expression of *C21orf91* is associated with genetic dependency on MITF in melanoma cell lines.

Table S3 – Upregulated genes associated with *PPP2R3B* expression are enriched for non-immune pathway signatures - transcriptomic data from 703 melanoma tumour samples from Leeds melanoma cohort (see methods for details)

Table S4 - Down regulated genes associated with *PPP2R3B* expression are enriched for immune pathway signatures - transcriptomic data from 703 melanoma tumour samples from Leeds melanoma cohort (see methods for details)

Table S5 – Pathway enrichment analysis from RNAseq of cell line inducible overexpression system for *PPP2R3B* (analysis excludes *PPP2R3B*), highlights suppression of the unfolded protein response and endoplasmic reticulum (ER) protein folding - comparison of pre- and post-induction samples in triplicate, at 6 and 16 hours post induction (see methods for details).

Table S6 - Reverse Phase Protein Array (RPPA) raw data from cell line inducible overexpression system for *PPP2R3B* demonstrates enrichment for mammalian target of rapamycin (mTOR) and hypoxia-induced factor 1 (HIF-1) signalling pathways, with prominent biological signatures of response to heat and stress - comparison of pre- and post-induction samples in triplicate, at 6 and 16 hours post-induction (see methods for details).

Table S7 - RNAseq data from cell line inducible overexpression system for *PPP2R3B*, significantly (Padj<0.05) differentially expressed genes in both cell lines in triplicate, at 6 and 16 hours post-induction (see methods for details). *C21orf91* was identified as the most significantly differentially expressed in both cell lines at both time points, other than *PPP2R3B*.

Supplementary

Melanoma Transcriptomic Data – Upregulated Pathways

The genes positively correlated with PPP2R3B are predominantly enriched in non-immune pathwaysm, consistent with the lack of association between PPP2R3B expression and TILs or any specific immune cell score. There are only 24 pathways significantly enriched in these genes at FDR<0.05 (Table below).

Using undirected interactions, the nodal genes in a network putting together all these pathways are: MAPK11 (betweenness=2237) and PLCB3 (betweenness=1120).

With directed interactions, the most important genes are MAPK11 (betweenness=103) and NFATC1 (betweenness=59).

Supplementary Table 3 - Melanoma Transcriptomic Data – Upregulated Pathways

Rank	Pathway	FDR
1	Rap1 signaling pathway(K)	6.10E-04
2	Axon guidance(K)	6.10E-04
3	ECM-receptor interaction(K)	9.94E-04
4	PI3K-Akt signaling pathway(K)	3.49E-03
5	DNA methylation(R)	5.66E-03
6	Pathways in cancer(K)	9.73E-03
7	Beta1 integrin cell surface interactions(N)	0.0157
8	Oxidative stress response(P)	0.0209
9	Arf1 pathway(N)	0.0281
10	Ras signaling pathway(K)	0.0281
11	Hedgehog signaling events mediated by Gli proteins(N)	0.0281
12	NoRC negatively regulates rRNA expression(R)	0.0281
13	EPH-Ephrin signaling(R)	0.0281
14	RNA Polymerase I Transcription(R)	0.0308
15	Signaling by VEGF(R)	0.035
16	MAPK signaling pathway(K)	0.0388
17	Focal adhesion(K)	0.0388
18	Endocytosis(K)	0.0388
19	Extracellular matrix organization(R)	0.0388
20	Shigellosis(K)	0.0463
21	EPHA forward signaling(N)	0.0463
22	DNA replication(P)	0.0498
23	Beta-catenin independent WNT signaling(R)	0.0498
24	Cell junction organization(R)	0.0528
25	Hedgehog signaling pathway(P)	0.054

Melanoma Transcriptomic Data – Downregulated Pathways

The genes negatively correlated with *PPP2R3B* expression are predominantly enriched in immune pathways. There are 80 pathways, the Table below shows the top 25.

Using undirected interactions, the top 5 nodal genes in a network putting together all these pathways are: TGFB1 (betweenness=8395) and AURKA (betweenness=5133) and CD8A (betweenness=4893), RAC2 (4880) and LCK (betweenness=4855).

With directed interactions, the most important genes are LCK (betweenness=174), HLA-G (betweenness=110), MYD88 (betweenness=104), TGFB1 (betweenness=86) and CD8A (betweenness=82).

Supplementary Table 4 - Melanoma Transcriptomic Data – Downregulated Pathways

Rank	Pathway	FDR
1	Natural killer cell mediated cytotoxicity(K)	3.50E-08
2	Antigen processing and presentation(K)	2.33E-07
3	Cytokine-cytokine receptor interaction(K)	2.33E-07
4	Immunoregulatory interactions between a Lymphoid and a non-Lymphoid cell(R)	5.45E-07
5	IL12-mediated signaling events(N)	6.57E-07
6	Malaria(K)	6.57E-07
7	Retinoid metabolism and transport(R)	6.57E-07
8	Graft-versus-host disease(K)	1.17E-06
9	IL12 signaling mediated by STAT4(N)	1.28E-06
10	Regulation of Insulin-like Growth Factor (IGF) transport and uptake by Insulin-like Growth Factor Binding Proteins (IGFBPs)(R)	1.81E-06
11	Cell adhesion molecules (CAMs)(K)	3.05E-06
12	Post-translational protein phosphorylation(R)	1.77E-05
13	Chemokine signaling pathway(K)	3.29E-04
14	G alpha (i) signalling events(R)	3.29E-04
15	Primary immunodeficiency(K)	4.49E-04
16	IL23-mediated signaling events(N)	4.49E-04
17	Osteoclast differentiation(K)	6.46E-04
18	Response to elevated platelet cytosolic Ca2+(R)	8.66E-04
19	Hematopoietic cell lineage(K)	1.02E-03
20	Th17 cell differentiation(K)	2.12E-03
21	TCR signaling in naive CD4+ T cells(N)	2.12E-03
22	African trypanosomiasis(K)	2.32E-03
23	TCR signaling in naive CD8+ T cells(N)	3.26E-03
24	Leishmaniasis(K)	3.28E-03
25	Extrinsic prothrombin activation pathway(B)	3.54E-03

Supplementary Table S5

Click here to access/download

Large Excel File

S3 RNAseq Pathway Enrichment.xls

Supplementary Table S6

Click here to access/download

Large Excel File

S4 Reverse Phase Protein Array Raw Data.xlsx

Supplementary Table S7

Click here to access/download

Large Excel File

S5 RNAseq Top Differentially Genes.xlsx

Source Data Supplemental Figure

Click here to access/download

Large Excel File

KINSLER-GIM-source-data-PPP-April2020.xlsx

Corresponding Author Name: VERONICA KINSLER
Manuscript Number: GIM-D-20-00465

Reporting Checklist* (Please see page 3 for instructions on uploading this file)

This checklist is used to ensure good reporting standards and to improve the reproducibility of published results. **Please respond completely to all questions relevant to your manuscript. For sections that are not applicable please fill in NA.** For more information, please read the journal's Guide to Authors.

⬓ Check here to confirm that the following information is available in the Material & Methods section:

- the **exact sample size (*n*)** for each experimental group/condition, given as a number, not a range;
- a **description of the sample collection** allowing the reader to understand whether the samples represent **technical or biological replicates** (including how many animals, litters, culture, etc.);
- a **statement of how many times the experiment shown was replicated in the laboratory**;
- **definitions of statistical methods and measures**: (For small sample sizes (n<5) descriptive statistics are not appropriate, instead plot individual data points)
    - very common tests, such as *t*-test, simple χ^2 tests, Wilcoxon and Mann-Whitney tests, can be unambiguously identified by name only, but more complex techniques should be described in the methods section;
    - are tests one-sided or two-sided?
    - are there adjustments for multiple comparisons?
    - **statistical test results**, e.g., ***P* values**;
    - definition of **'center values'** as **median or mean**;
    - definition of **error bars as s.d. or s.e.m. or c.i.**

Please ensure that the answers to the following questions are reported both **in the manuscript itself and in the space below.** We encourage you to include a specific subsection in the methods section each for statistics, reagents and animal models. Below, provide the text as it appears in the manuscript as well as the page number.

Statistics and general methods	**Text AND page number from manuscript**
1. How was the sample size chosen to ensure adequate power to detect a pre-specified effect size? (Give text and page #)	NA
For animal studies, include a statement about sample size estimate even if no statistical methods were used.	NA
2. Describe inclusion/exclusion criteria if samples or animals were excluded from the analysis. Were the criteria pre-established? (Give text and page #)	NA
3. If a method of randomization was used to determine how samples/animals were allocated to experimental groups and processed, describe it. (Give text and page #)	NA
For animal studies, include a statement about randomization even if no randomization was used.	NA

4. If the investigator was blinded to the group allocation during the experiment and/or when assessing the outcome, state the extent of blinding. (Give text and page #)	NA
For animal studies, include a statement about blinding even if no blinding was done.	Yes
5. For every figure, are statistical tests justified as appropriate?	Yes
Do the data meet the assumptions of the tests (e.g., normal distribution)?	Yes
Is there an estimate of variation within each group of data?	Yes
Is the variance similar between the groups that are being statistically compared? (Give text and page #)	Yes

Reagents	**Text AND page number from manuscript**
6. Report the source of antibodies (vendor and catalog number)	Yes, supplementary, page 6
7. Identify the source of cell lines and report if they were recently authenticated (e.g., by STR profiling) and tested for mycoplasma contamination	Yes, supplementary

Animal Models	**Text AND page number from manuscript**
8. Report species, strain, sex and age of animals	NA
9. For experiments involving live vertebrates, include a statement of compliance with ethical regulations and identify the committee(s) approving the experiments.	NA

10. We recommend consulting the ARRIVE guidelines (*PLoS Biol.* **8**(6), e1000412,2010) to ensure that other relevant aspects of animal studies are adequately reported.

Human subjects	**Text AND page number from manuscript**
11. Identify the committee(s) approving the study protocol.	Yes, supplementary, page 6
12. Include a statement confirming that informed consent was obtained from all subjects.	Yes, supplementary, page 6
13. For publication of patient photos, include a statement confirming that consent to publish was obtained. For more information, please see http://www.icmje.org/recommendations/browse/roles-and-responsibilities/protection-of-research-participants.html.	NA
14. Report the clinical trial registration number (at ClinicalTrials.gov or equivalent).	NA

15. For phase II and III randomized controlled trials, please refer to the CONSORT statement and submit the CONSORT checklist with your submission.

16. For tumor marker prognostic studies, we recommend that you follow the REMARK reporting guidelines.

Data deposition	**Text AND page number from manuscript**
17. Provide accession codes for deposited data. Data deposition in a public repository is recommended for: a. Protein, DNA and RNA sequences b. Macromolecular structures c. Crystallographic data for small molecules d. Microarray data	Yes, page 17

Deposition is strongly recommended for many other datasets for which structured public repositories exist; more details on our data policy are available in the Guide to Authors. We encourage the provision of other source data in supplementary information or in unstructured repositories such as Figshare and Dryad. We encourage publication of Data Descriptors (see Scientific Data) to maximize data reuse.

18. If computer code was used to generate results that are central to the paper's conclusions, include a statement in the Methods section under "**Code availability"** to indicate whether and how the code can be accessed. Include version information as necessary and any restrictions on availability.	NA

* If an error is shown on the PDF built in Editorial Manager after including this Reporting Checklist take the following steps:
1. Open the original filled GIM-reporting-checklist.pdf with Mac Preview App
2. Goto Tray -> Export as PDF
3. Save as: at your desk (local computer) with a different file name
4. Close the app
5. In Editorial Manager: Edit the Submission which displayed Error or Incomplete Status and remove the file, then upload the new one, and again select to build the merged PDF

Genetics in Medicine ARTWORK FORM

This form must be completed for all papers. We will be unable to process your paper through to production until we receive instructions concerning color files.

MANUSCRIPT NUMBER__GIMD-20-00465R3

Artwork Quality Checklist (must be completed as applicable)

Please refer to our publisher's artwork guidelines for further details:

☒ My files are in the correct format – PDF, EPS, or AI file format at 300 dpi or higher resolution

☒ My color images are provided in RGB color mode

☒ All figures are provided as separate files.

☒ All artwork is numbered according to its sequence in the text.

☒ Figures, schemes, and plates have titles and separate captions/legends and these are provided within the manuscript

☒ All figures are referred to in the text.

☒ For microscope images, I have included a scale bar on the image and stated in the figure legend what length the scale bar represents.

Does your article contain figures that must be printed in color? Yes ☒ No ☐
If yes:

Color Figure Charges:

$500 for the first color figure and $250 for each subsequent figure. Current ACMG members (excluding Student Members) who are first or senior/corresponding authors are exempt,* as are authors who have opted for Open Access.*
Please note that figures can appear online in color in the HTML version of your manuscript, and in black and white in the PDF/print version of the manuscript. Color figures will also be at the discretion of the editorial office. The option to publish Open Access will be offered through our publisher's self-service platform following the editorial office's transmission of your article to production.

Please check:

☒ Yes, my manuscript contains material that must be printed in color. I agree to pay the color charges in full and hereby authorize Springer Nature to invoice me for the cost of reproducing color artwork in print.

☐ Yes, my manuscript contains material that should be in color in the online HTML version, but in black and white in the PDF/print version of the manuscript. No charges incurred.

☐ Yes, my manuscript contains material that must be printed in color, but I am an ACMG member, so am exempt. No charges incurred. Eligible College Member's Name:

_____
Membership will be verified by the Editorial Staff and false claims will be liable for the full color charge rate.